Numerical Analysis of a Mediterranean "Hurricane" over Southeastern Italy

AGATA MOSCATELLO AND MARIO MARCELLO MIGLIETTA
ISAC-CNR, Lecce, Italy

RICHARD ROTUNNO
National Center for Atmospheric Research, Boulder, Colorado*

(Manuscript received 27 December 2007, in final form 26 March 2008)

ABSTRACT

The presence of a subsynoptic-scale vortex over the Mediterranean Sea in southeastern Italy on 26 September 2006 has been recently documented by the authors. The transit of the cyclone over land allowed an accurate diagnosis of the structure of the vortex, based on radar and surface station data, showing that the cyclone had features similar to those observed in tropical cyclones. To investigate the cyclone in greater depth, numerical simulations have been performed using the Weather Research and Forecasting (WRF) model, set up with two domains, in a two-way-nested configuration. Model simulations are able to properly capture the timing and intensity of the small-scale cyclone. Moreover, the present simulated cyclone agrees with the observational analysis of this case, identifying in this small-scale depression the typical characteristics of a Mediterranean tropical-like cyclone. An analysis of the mechanisms responsible for the genesis, development, and maintenance of the cyclone has also been performed. Sensitivity experiments show that cyclogenesis on the lee side of the Atlas Mountains is responsible for the generation of the cyclone. Surface sensible and latent heat fluxes become important during the subsequent phase of development in which the lee-vortex shallow depression evolved as it moved toward the south of Sicily. During this phase, the latent heating, associated with convective motions triggered by a cold front entering the central Mediterranean area, was important for the intensification and contraction of the horizontal scale of the vortex. The small-scale cyclone subsequently deepened as it moved over the Ionian Sea and then maintained its intensity during its later transit over the Adriatic Sea; in this later stage, latent heat release continued to play a major role in amplifying and maintaining the vortex, while the importance of the surface fluxes diminished.

1. Introduction

It is well known that the western Mediterranean Sea is an important cyclogenetic area (for a recent review of the observational literature, see Campins et al. 2006). As the Mediterranean Sea is bordered by long and tall mountain chains, orographic lee cyclogenesis [Buzzi and Tibaldi (1978); for reviews see Pierrehumbert (1984), or more recently, Davis and Stoelinga (1999)] is often implicated in the formation of cyclones in this area. It is also true that, being a large and sometimes warm body of water, the Mediterranean Sea can be an area of cyclogenesis influenced by convective instability and air–sea interaction, producing cyclones with some of the characteristics of hurricanes (Billing et al. 1983; Ernst and Matson 1983; Rasmussen and Zick 1987). In the present study, numerical simulations of the hurricane-like cyclone over southern Italy on 26 September 2006 are analyzed to provide a plausible explanation of how the combination of lee cyclogenesis, convective instability, and air–sea interaction produced the observed cyclone.

There have been a number of recent case studies of hurricane-like cyclones in the Mediterranean. In almost all observed cases convective instability is shown to play an important role. Case-to-case differences arise with respect to the role of upper-level precursors and orography. For example, Reale and Atlas (2001) described two small-scale cyclones with tropical-like characteristics that occurred over the western and central Mediterranean, showing the importance of the upper-

* The National Center for Atmospheric Research is sponsored by the National Science Foundation.

Corresponding author address: Agata Moscatello, Institute of Atmospheric Sciences and Climate (ISAC-CNR), Strada Provinciale km 1, 200, 73100 Lecce, Italy.
E-mail: agata@le.isac.cnr.it

DOI: 10.1175/2008MWR2512.1

level forcing for the low-level cyclogenesis. Similarly, Romero (2001) and Homar et al. (2002, 2003) examined the role of finer-scale, upper-level potential vorticity anomalies in initiating small-scale cyclones in the western Mediterranean; the role of orography was found in these studies to be minimal. Fita et al. (2007) characterized the environments in which seven different Mediterranean tropical-like cyclones developed, pointing out the importance of the sea surface temperature, the initial vertical temperature and humidity profile, and size of the initial upper-level precursors (e.g., potential vorticity anomalies) present in the synoptic-scale flow.

As mentioned above, the importance of convective instability has been cited in all case studies of hurricane-like cyclones in the Mediterranean; the means by which convective instability is produced has been the subject of many numerical studies examining the role of fluxes of heat and moisture from the Mediterranean Sea. Pytharoulis et al. (2000) performed numerical experiments illustrating that both the surface fluxes of heat and moisture are fundamental for this type of hurricane-like cyclogenesis and are important and comparable during the subsequent development of the cyclone. Sensitivity simulations, carried out by Lagouvardos et al. (1999) for the same case study, stressed the role played by the fluxes in the formation of the storm and the strong influence of the latent heat release associated with convective motions during its mature stage. Emanuel (2005) hypothesized that a hurricane-like cyclone can intensify within observed environments by a process analogous to that demonstrated in simulations of tropical cyclones.

The present study concerns an intense, small-scale (~60-km diameter) cyclone that affected southeastern Italy on 26 September 2006. An observational analysis of the cyclone was performed by the authors (Moscatello et al. 2008, hereafter MMR08) revealing that the cyclone possessed features typical of tropical cyclones. In the present paper, our observational study of the event is complemented with the analysis of numerical simulations thereof. As the present simulations agree very well with the available data, one can reasonably expect the simulations to provide a surrogate dataset with which to examine the mechanisms responsible for the genesis, development, and maintenance of the cyclone. In the present case, we find that orography, surface heat and moisture fluxes, and latent heat release play important roles in the different phases of evolution of the simulated cyclone. The analysis of these processes forms the body of the current work. Section 2 gives a summary of the observational evidence of the event, as described in MMR08. Section 3 describes the characteristics of the model used for this study and the numerical setup employed for the control run and for the sensitivity experiments. Section 4 discusses the control run results, showing that the model is able to realistically simulate the evolution of the system. Section 5 is focused on the analyses of the sensitivity studies, aimed at understanding the mechanisms at work during the different phases of the life of the vortex. A final discussion and conclusions are presented in section 6.

2. Summary of the observational analysis

The presence of a subsynoptic-scale vortex that formed over the Mediterranean Sea and affected southeastern Italy on 26 September 2006 has been documented by the authors (MMR08). Radar maps, satellite images, and surface station data were used to detect the main features of the vortex and its trajectory from the time the cyclone crossed the southern part of Apulia, Italy (the Salentine peninsula; see Fig. 1) to its decay in the northern part of the region after passing over the Adriatic Sea.

At 0600 UTC 26 September, the European Centre for Medium-Range Weather Forecasts (ECMWF) analyses reveal (Fig. 2 of MMR08) the presence of two areas of low pressure over the Italian peninsula: the first one, with a minimum pressure of approximately 1001 hPa approaches the central Tyrrhenian (west) coast from the west; the second one, of smaller horizontal scale and with a deeper pressure minimum of 998 hPa, is located over the northern Ionian Sea and rotates around the Tyrrhenian minimum (see its trajectory in Fig. 1).

The low space and time resolution of the ECMWF analyses does not allow for the representation of the mesoscale pressure minimum over the Ionian Sea with its correct intensity or an accurate reproduction of its path. Higher-resolution analyses were done in MMR08 using data provided every 15 min from a meso-network of 33 surface stations distributed in Apulia. The results showed that the vortex had a horizontal extent of about 60 km, crossed the Salentine peninsula (~40 km wide) from south-southwest to north-northeast in about 30 min, and reached a sea level pressure minimum of 986 hPa at 0915 UTC.

The pressure gradient associated with the small-scale cyclone was very large, approximately 10 hPa $(20\ \text{km})^{-1}$, and wind gusts exceeding 78 kt were observed during its passage across Salento. Radar reflectivity maps are consistent with this analysis, showing the absence of precipitation near the pressure minimum, as a consequence of the passage of the "eye" of the cyclone through the region (Fig. 5 of MMR08).

After approximately 1000 UTC 26 September, both

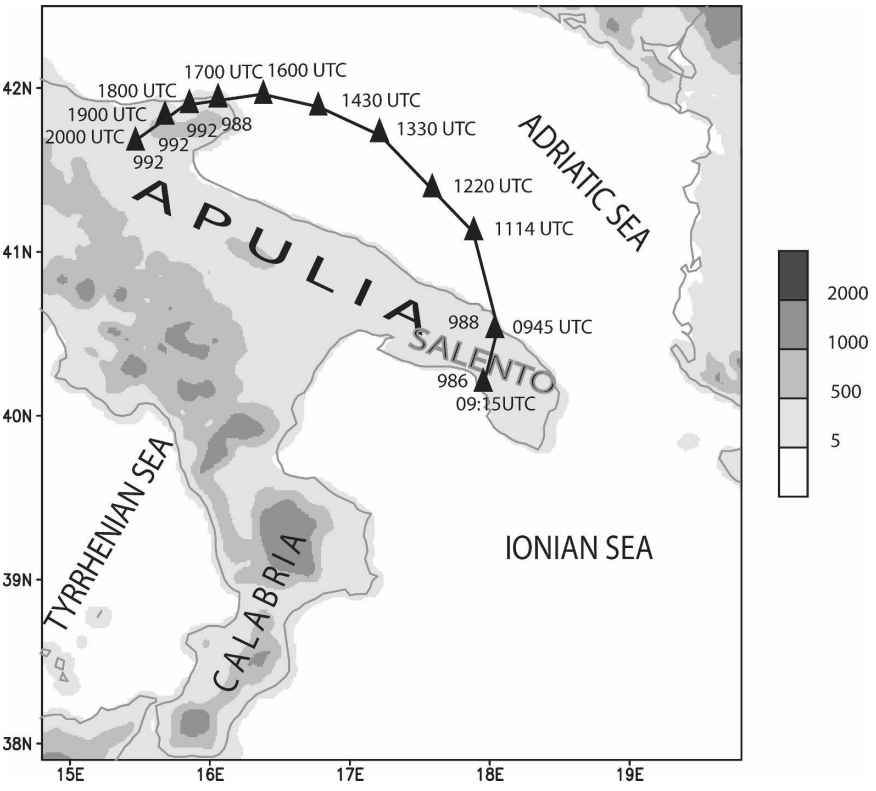

FIG. 1. The best estimate of the track of the Mediterranean cyclone between approximately 0915 and 2000 UTC 26 Sep 2006, as reconstructed from the observational data. The numbers on the left side of the track denote the minimum values of the MSLP (hPa) at each point; the time of the passage of the pressure low at each point is denoted on the right side of the track.

the radar maps and the Meteosat Second Generation satellite images showed the passage of the vortex over the Adriatic Sea and its movement northwestward (Fig. 1). Around 1700 UTC 26 September, the cyclone moved inland and was still very deep, with a pressure minimum of about 988 hPa recorded in the northern part of the region at 1700 UTC. Sometime after 2000 UTC 26 September, the minimum mean sea level pressure (MSLP) began to increase as the cyclone moved farther inland toward the west-southwest, where it finally decayed (Fig. 1).

By collecting all the available observations, MMR08 determined the full track of the cyclone and pointed out the main features of the system. As revealed by their observational analysis, the vortex possessed characteristics typical of tropical cyclones, such as a spiral shape; an evident eyelike feature; a deep, rapid pressure fall; and a strong surface wind, with the strongest wind found in the vortex eyewall.

3. Model description and setup

The model used in this study is the Weather Research and Forecasting (WRF) Model, version 2.2 (Skamarock et al. 2005; Michalakes et al. 2004; see also http://www.wrf-model.org/index.php). The model solves the fully compressible, nonhydrostatic Euler equations. Terrain-following hydrostatic pressure vertical coordinates are used and the top of the model is a constant pressure surface. A time-split integration method using a third-order Runge–Kutta scheme is utilized (Wicker and Skamarock 2002), with smaller time steps for acoustic and gravity waves modes. In the setup adopted here, the fifth-order advection scheme is employed in the horizontal and the third-order scheme is employed in the vertical.

The model integration domain is shown in Fig. 2; it has a horizontal grid spacing of 16 km and covers approximately the central and the western Mediterranean regions, including northern Africa, Spain, and the Italian peninsula. The grid is centered at 39°N, 5°E and has 216 × 138 horizontal grid points. Depending on the phase of the event focused on, different locations were selected for the inner grid nest. Thus, in some numerical experiments the inner domain covers southern Italy and the surrounding seas ("G2a" in Fig. 2), while in other experiments the inner grid is centered over the

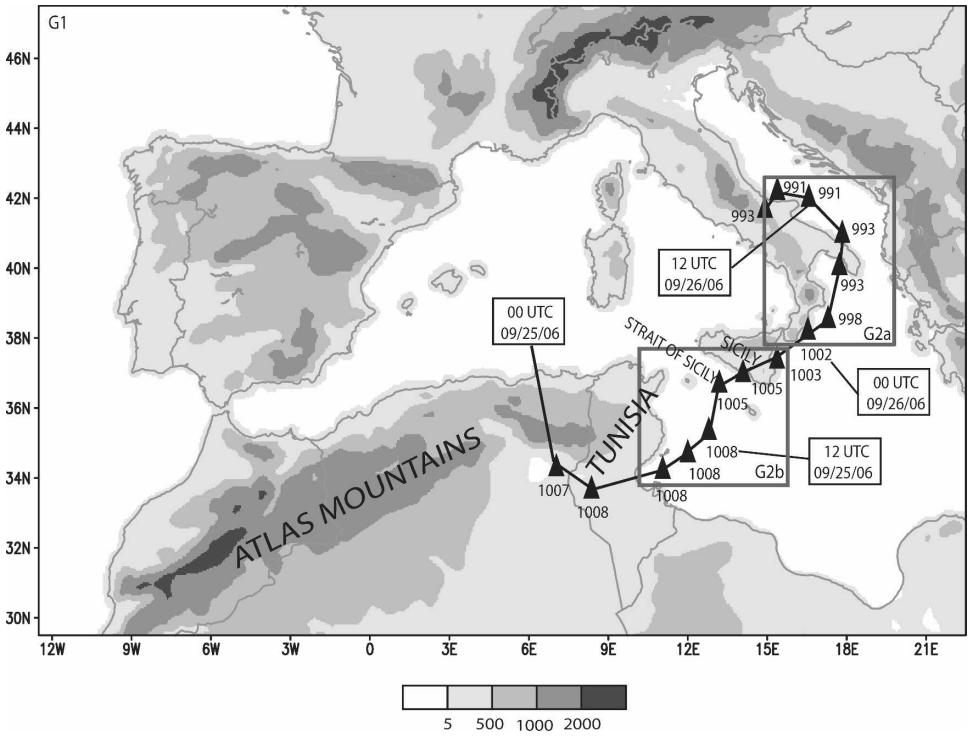

FIG. 2. Control run (coarse grid): Track of the cyclone from 0000 UTC 25 Sep to 1800 UTC 26 Sep (black triangles indicate the position of the minimum every 3 h). The numbers denote the minimum values (hPa) of the mean sea level pressure. The model topography (m) is represented with grayscale-shaded areas. The rectangular boxes indicate the two different nested grids used in the numerical experiments.

central Mediterranean Sea, between southern Sicily and the Tunisian coast ("G2b" in Fig. 2). In both configurations, the inner grid has a horizontal resolution of 4 km and is nested into the main domain using a two-way nesting technique. Thirty terrain following hydrostatic vertical levels are used for both grids, with enhanced vertical resolution of about 100 m in the lower atmosphere.

A full set of parameterizations is included in the model for microphysics, convection, turbulence, soil processes, boundary layer processes, and radiation. In the model configurations used here, the following parameterizations have been selected: the Thompson et al. (2004) microphysics, which includes six classes of moisture species plus number concentration for ice as prognostic variables; the Kain (2004) cumulus parameterization (on the coarser grid; no parameterization is used on the inner finer grids); the Rapid Radiative Transfer Model (RRTM) for longwave radiation, based on Mlawer et al. (1997); the Dudhia (1989) scheme for shortwave radiation; the Yonsei University (YSU) scheme for the boundary layer (Hong and Pan 1996); the surface layer parameterization based on the stability functions from Paulson (1970), Dyer and Hicks (1970), and Webb (1970); and a five-layer thermal-diffusion soil scheme (Skamarock et al. 2005).

In choosing the setup ultimately used for this study, different model configurations were tested by changing the dimensions of the domains, the starting time, the type of analyses, etc. Although most of these simulations were able to reproduce the evolution of the cyclone, a significant sensitivity was found, regarding both the exact position of the vortex and the intensity of the pressure minimum. A detailed description of this sensitivity analysis is outside the scope of the present paper, but see Davolio et al. (2008, manuscript submitted to *Nat. Hazards Earth Syst. Sci.*) for a multimodel multianalysis approach to the present case study. In the present study, the configuration chosen for the control run was the one that best reproduced the observed cyclone characteristics.

4. Evolution of the cyclone in control simulation coarse grid

A set of numerical simulations has been performed in order to reproduce the observed development of the cyclone and to understand the mechanisms involved in its different phases. The full list of experiments is shown

TABLE 1. Configuration of the different numerical experiments: 1 indicates that the factor, shown in the top row, is activated during the simulation and 0 indicates that is switched off. G2a and G2b refer to the two different nested grids used in the numerical experiments; their location with respect to the main domain is shown in Fig. 2.

Expt	Atlas orography	Latent heat	Surface fluxes	Inner grid	Restart run	Simulated period
Control run	1	1	1	G2a	No	0000 UTC 24 Sep–0000 UTC 27 Sep
EXP-1	0	1	1	G2a	No	0000 UTC 24 Sep–0000 UTC 27 Sep
EXP-2	1	1	1	G2b	No	0000 UTC 24 Sep–0000 UTC 26 Sep
EXP-3	1	0	1	G2b	Yes	0000 UTC 25 Sep–0000 UTC 26 Sep
EXP-4	1	1	0	G2b	Yes	0000 UTC 25 Sep–0000 UTC 26 Sep
EXP-5	1	0	1	G2a	Yes	0000 UTC 26 Sep–0000 UTC 27 Sep
EXP-6	1	1	0	G2a	Yes	0000 UTC 26 Sep–0000 UTC 27 Sep
EXP-7	1	0	1	G2a	Yes	0600 UTC 26 Sep–0000 UTC 27 Sep
EXP-8	1	1	0	G2a	Yes	0600 UTC 26 Sep–0000 UTC 27 Sep

in Table 1. In the present section, the results of the control run are discussed. In this experiment, the inner grid has 129 × 149 grid points in the horizontal and covers the area (G2a in Fig. 2 is shown in more detail in Fig. 1) where the vortex had its strongest intensity. The simulation started at 0000 UTC 24 September 2006 and lasted for 72 h. Initial conditions were provided by the 0.5° × 0.5° ECMWF analyses. These analyses were also used to update the lateral boundary conditions on the large domain every 6 h.

The results of the numerical simulation on the coarse domain are discussed here. As a consequence of mechanisms that will be discussed below, Fig. 2 shows that a small-scale cyclone is generated south of the Atlas Mountains at around 0000 UTC 25 September. Figure 2 shows the subsequent evolution of the small-scale depression for 42 h of simulation. From its initial appearance at 1200 UTC 24 September, and for the following 12 h, the system neither moves significantly nor deepens. At approximately 0000 UTC 25 September, the surface low begins moving eastward under the influence of an upper-level trough to its northwest (not shown), without intensifying, and reaches the Mediterranean Sea, east of Tunisia, at 0600 UTC 25 September as shown in Fig. 2. Subsequently, Fig. 2 shows that the pressure minimum deepens slightly (from 1008 to 1003 hPa in 15 h) as it moves across the Strait of Sicily; the track is oriented north-northeastward in the morning, and then northeastward during the evening, as the cyclone's track was probably influenced by the mountainous island of Sicily.

During the same period, the main upper-level trough deepens as it reaches the Tyrrhenian Sea (not shown). At 0000 UTC 26 September, the surface cyclone enters the Ionian Sea, approaching the Ionian coast of Calabria, Italy. At this time, the vortex moves in a south-southwest to north-northeast direction and quickly intensifies, reaching a minimum value of 993 hPa at 0600 UTC near the western coast of the Salentine peninsula. Figure 2 shows that in the following hours, the cyclone crosses Salento rapidly and moves along the southern Adriatic Sea, curving strongly toward the northwest in apparent response to a surface low pressure system on the Tyrrhenian (west) coast (not shown). During its passage over the sea, the pressure minimum remains almost constant around 991–993 hPa; after 1200 UTC 26 September, the system approaches the northern part of Apulia and ultimately moves inland, where the pressure minimum slowly increases and the vortex decays. Comparing the trajectory shown in Fig. 2 with that of Fig. 1, it is clear that the control simulation well predicts the observed trajectory (at least during the well-documented final phase), although it overestimates the value of the pressure minimum by a few hectopascals.

To obtain a more accurate description of the vortex evolution, we next consider in more detail the results from the inner high-resolution grid. Figure 3a shows the trajectory followed by the cyclone along the Ionian Sea and the Adriatic Sea, until its final decay inland, in the northern part of the region; the best estimation of the cyclone track, as presented in Fig. 1, is also shown (dashed line). The finer resolution allows for a more detailed description of the intensity of the cyclone and of its trajectory and so the points identifying the position of the pressure minimum are reported in Fig. 3a every 1 h instead of every 3 h as for the coarser grid.

As illustrated in Fig. 3a, the model indicates a large pressure fall of 13 hPa in 7 h, during the transit of the vortex over the Ionian Sea (there is no documentation of this from the observations, however), from 0000 to 0700 UTC 26 September, with a maximum drop of 7 hPa from 0300 to 0400 UTC. The model predicts the movement of the cyclone across the Salentine peninsula from 0700 to 0800 UTC; during this phase, the model forecasts the MSLP of 989 hPa, which is the lowest simulated value, occurring along the southern side of the peninsula. After its quick (1 h) transit over land, the pressure minimum increases to a value of 992 hPa. Dur-

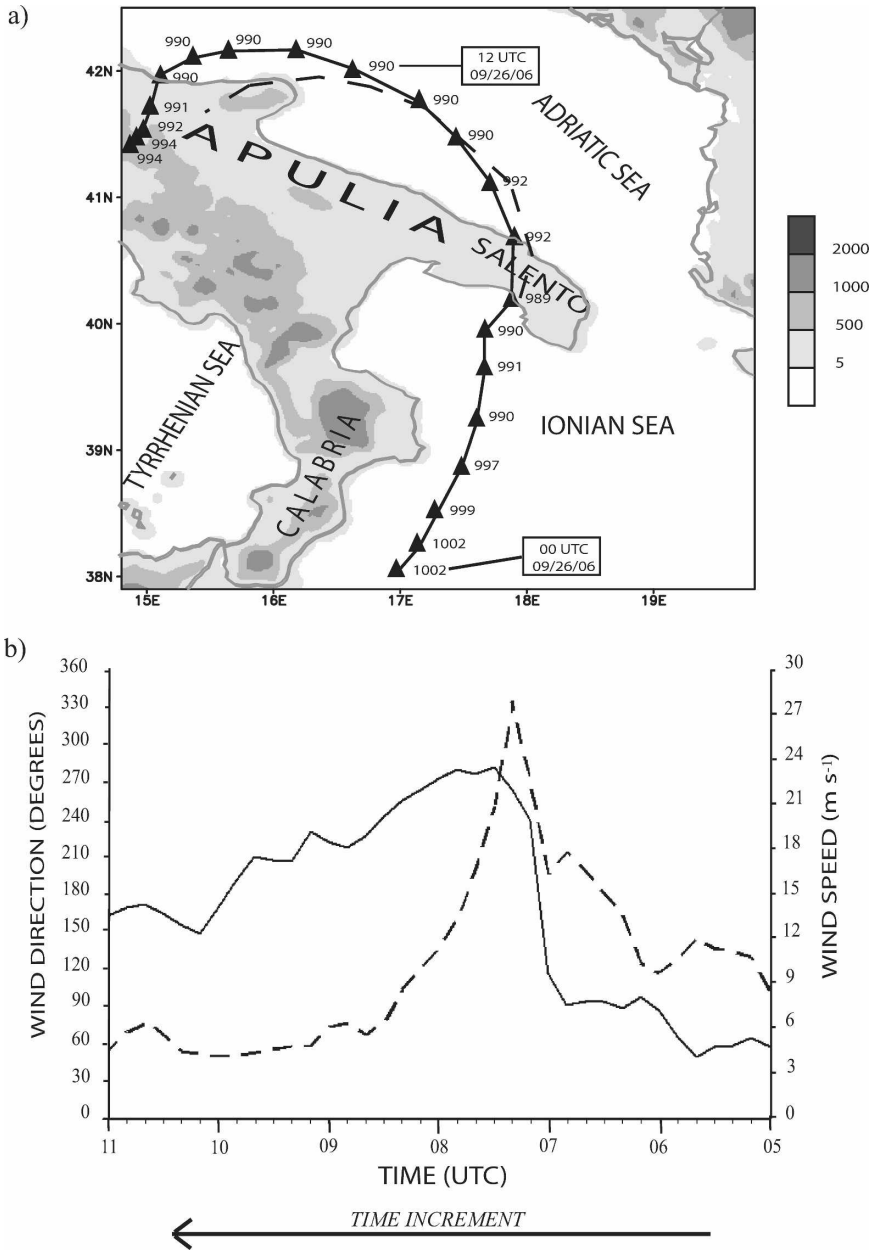

FIG. 3. Control run (inner grid): (a) as in Fig. 2, except that the track of the cyclone is shown from 0000 to 2000 UTC 26 Sep and the black triangles indicate the position of the cyclone every 1 h; the best estimate of the track, as shown in Fig. 1, is superimposed (dashed line). (b) Wind direction (solid line) and wind speed (dashed line) simulated at the grid point closest to Galatina airport from 0500 to 1100 UTC.

ing the subsequent movement across the Adriatic Sea, the pressure minimum decreases again, reaching the value of 990 hPa, and remains constant until the second landfall of the vortex at 1600 UTC, in the northern part of Apulia. In the following hours, the pressure center fills, as the vortex moves inland toward the west-southwest.

Comparing the observed with the simulated trajectory (Fig. 1 versus Fig. 3a), it is apparent that there is a good agreement between the model simulations and the observations, although the arrival of the simulated cyclone inland precedes that of the observed cyclone by 2 h. In fact, according to the radar data (Fig. 5 of MMR08), the vortex approaches the Salentine peninsula at 0840 UTC, whereas in the control run the landfall occurs at about 0700 UTC. Also, the track of the

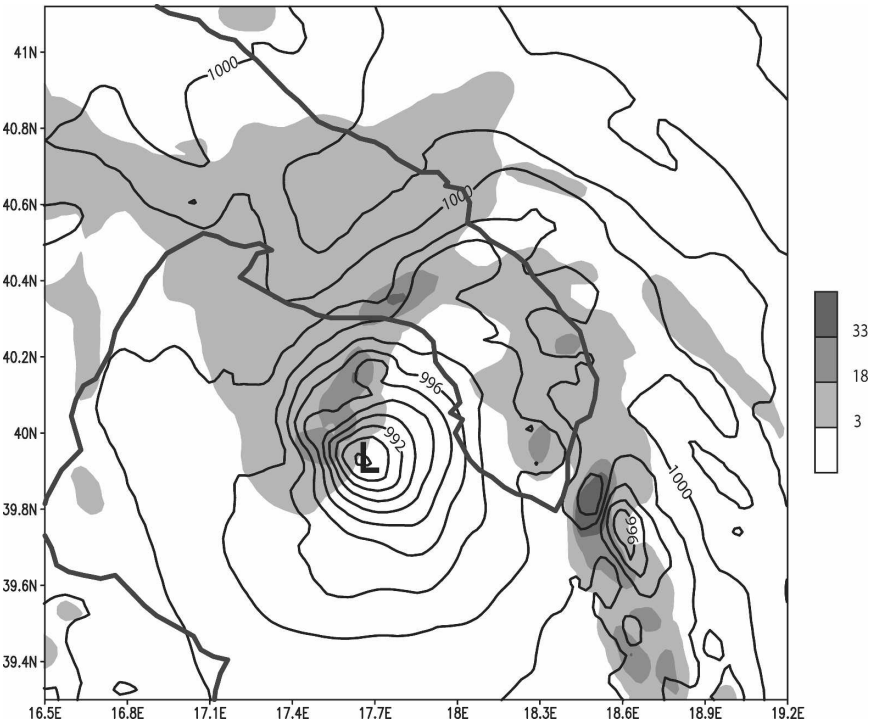

FIG. 4. Control run (inner grid): Rainwater (g kg^{-1}) at the 800-hPa pressure level (grayscale-shaded areas) and MSLP [black contours, contour interval (CI) = 1 hPa] at 0600 UTC 26 Sep; the position of the vortex is denoted by an "L."

simulated cyclone is slightly shifted to the west in the morning and to the north in the evening with respect to the observed trajectory (see dashed and solid lines in Fig. 3), but the overall agreement is satisfactory. The model also well simulates the pressure minimum values: the lowest pressure value of 986 hPa observed on the Salentine peninsula (Fig. 6 of MMR08) is approximately reproduced by the model (the simulated minimum value is 989 hPa); similarly, the minimum of 988 hPa registered in northern Apulia after the cyclone moves inland in the evening (Fig. 6 of MMR08) is well simulated (the model value is 990 hPa). The wind direction and speed simulated at the grid point closest to Galatina (the location of the observations reported in Fig. 7 of MMR08) are shown in Fig. 3b. A comparison of Fig. 3b with MMR08's Fig. 7 shows that the model is able to reproduce the rotation of the wind from east to west and then to south after the passage of the cyclone (although with a 2-h delay). The intensities of the two wind maxima are also reduced (the simulated maximum is about 28 m s^{-1}, i.e., about 50 kt, while the observed value was 78 kt), mainly as a consequence of the relatively low resolution employed in the experiments, which is not able to reproduce correctly the smaller-scale features of the vortex.

In conclusion, compared to the coarse-domain simulation, the finer-grid simulation significantly improves the agreement of the simulated cyclone's intensity and evolution with respect to observations. The control run can thus be considered accurate enough to provide a reasonable complementary dataset for further diagnosis and analysis of the observed cyclone.

Figure 4 shows the simulated cyclone during its mature phase, when the vortex is well formed and is approaching the Salentine peninsula. At this time (0600 UTC 26 September) the observations show (see Figs. 2, 5, and 7 of MMR08) that the system had features typical of tropical cyclones, such as the spiral cloud structure, strong convection, and strong low-level winds—features that the model is able to reproduce well. In fact, Fig. 4 shows a strong pressure gradient around the cyclone center, associated with strong surface winds around the vortex center (not shown), and a rainwater content at 800 hPa formed in a spiral shape around the pressure minimum, with a broad band of rainwater on the northern flanks of the vortex, while the southern flank is free of precipitation (similar to that found in Lagouvardos et al. 1999). This structure is similar to the convective rainbands observed around the eye in the radar reflectivity fields shown in Fig. 5b of MMR08. The temperature at 800 hPa shows a maximum above the vortex (not shown), indicating that the vortex pos-

sesses a warm-core structure, as expected based on the typical structure of tropical-like cyclones in the Mediterranean Sea (Lagouvardos et al. 1999; Pytharoulis et al. 2000).

5. Sensitivity studies

The analysis of the cyclone in the control run evidenced four different phases in its life cycle (Fig. 2):

phase 1: cyclone formation in northern Africa;
phase 2: passage of the cyclone across the Strait of Sicily (between Tunisia and Sicily);
phase 3: transit of the cyclone over the Ionian Sea and first landfall over the Salentine peninsula; and
phase 4: transit of the cyclone over the Adriatic Sea and a second landfall in the northern part of Apulia.

In this section, we will analyze the main factors responsible for the formation of the cyclone and the mechanisms that led to its intensification in the different phases. We will first analyze the results of the control run in more detail in order to have a general overview of the synoptic situation before going on to an analysis of the small-scale vortex.

a. Control run

At 0000 UTC 24 September, two days before the event affected Apulia, the large-scale flow (not shown), as simulated by the model (and in agreement with the ECMWF analysis), is characterized by a deep trough that extends from the Atlantic Ocean toward North Africa. Figure 5a shows that by 1200 UTC 24 September, a trough at 500 hPa, with its axis tilted south-southeast–north-northwest, enters the western Mediterranean basin. The eastward progression of the trough implies developing northerly winds over the Atlas Mountains with southwesterlies ahead of it to the east. Figure 5b shows that at 850 hPa there is an associated cold front progressing southward and eastward and hence impinging upon the Atlas Mountains.

Figure 6 shows the evolution of the MSLP and the 850-hPa wind in the control run on the coarse domain, from 1800 UTC 24 September to 1200 UTC 25 September, which we designate as phase 1. A pressure minimum of 1005 hPa is clearly visible to the southeast of the Atlas Mountains in Fig. 6a; in this phase, west-northwesterly synoptic flow impinges on the orography. Subsequently at 1200 UTC 25 September, Fig. 6b shows that the cyclone has moved eastward over the sea, with a minimum pressure value of 1008 hPa.

The vertical distribution of potential temperature and of the north–south wind component in the region around the vortex are illustrated in Figs. 6c,d, which

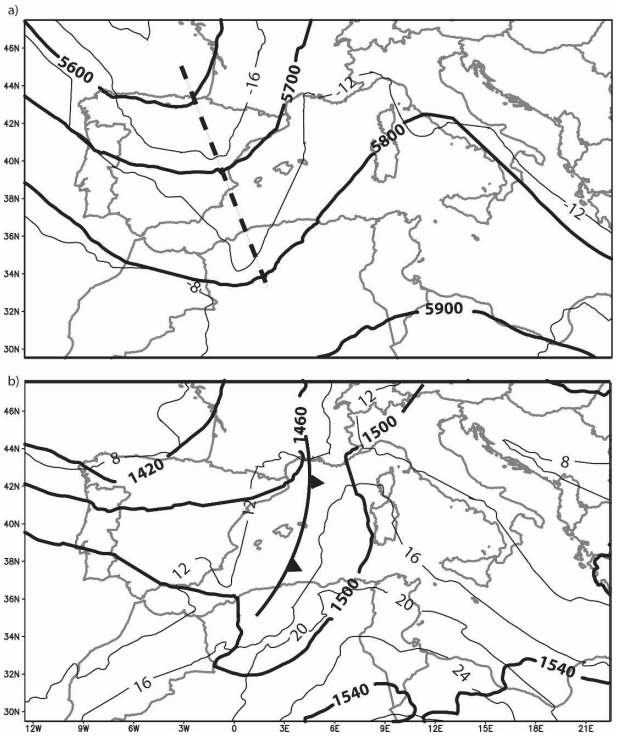

FIG. 5. Control run (coarse grid): (a) 500-hPa geopotential height (thick solid contours, CI = 100 m), 500-hPa temperature field (thin solid contours, CI = 4°C), and trough axis (dashed black line) at 1200 UTC 24 Sep; (b) 850-hPa geopotential height (thick solid contours, CI = 40 m), 850-hPa temperature field (thin solid contours, CI = 4°C), and the position of the frontal system at 1200 UTC 24 Sep.

correspond respectively to cross sections along the line AA′ shown in Figs. 6a,b. Figures 6c,d illustrate the passage of air from the top of the mountain toward its lee side, producing a stretching of the air column and consequently strong cyclonic vorticity [an example of "transient generation" as described in section 21.5 of Pierrehumbert (1984); see also Skamarock et al. (1999)] immediately downwind of the Atlas Mountains. This is not a rare event, as the climatology in Fig. 6b of Campins et al. (2006) shows that this area is near the climatological maximum for the production of shallow cyclones. After its lee-side generation, the vortex subsequently moves over the open sea (Figs. 6b,d), maintaining a strong circulation, especially in the lowest levels. The mechanisms involved in the further intensification and contraction of the cyclone are complex and will be detailed below along with sensitivity experiments to test the roles of the various processes involved.

b. Experimental configuration

Table 1 contains a description of eight additional experiments performed to investigate further the mecha-

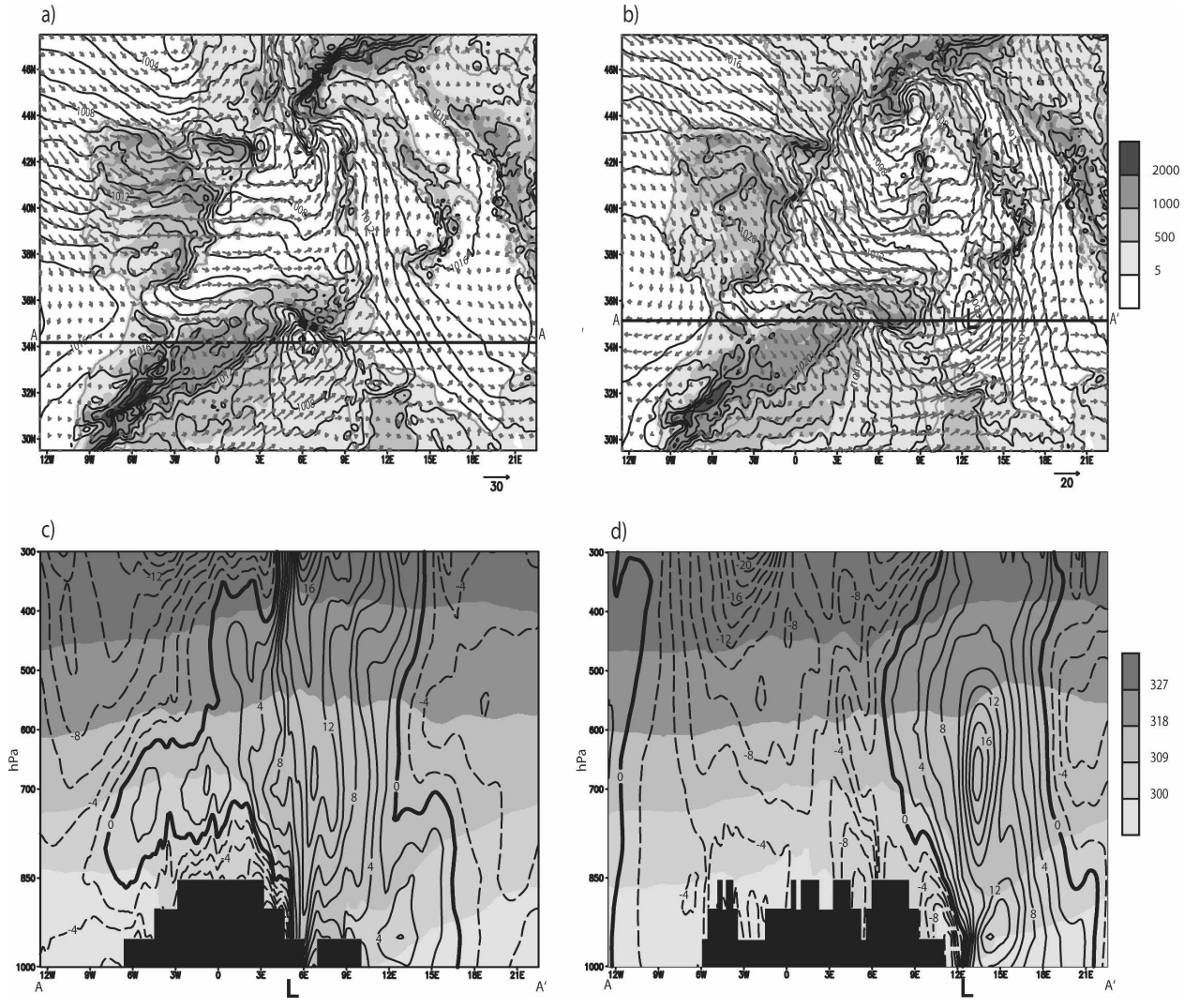

FIG. 6. Control run (coarse grid): MSLP (black contours, CI = 1 hPa) and 850 hPa-horizontal wind (gray arrows) at (a) 1800 UTC 24 Sep and (b) 1200 UTC 25 Sep [the bold horizontal line AA′ in (a) and (b) denotes the location of the cross sections represented in (c) and (d)]; potential temperature (K, grayscale-shaded areas) and V wind component (contours in m s^{-1}, CI = 2 m s^{-1}) along the vertical cross sections AA′ at (c) 1800 UTC 24 Sep and (d) 1200 UTC 25 Sep. The "L" at the bottom of the panels represents the position of the cyclone. In (a) and (b), the model topography is represented with grayscale-shaded areas, and the 850-hPa wind speed is proportional to the length of the arrows: the unit length is shown on the bottom-right side of each panel and is equal to 30 m s^{-1} in (a) and 20 m s^{-1} in (b).

nisms responsible for the evolution of the simulated cyclone during the four phases identified above. To test the importance of the Atlas Mountains in producing a lee-side cyclone (phase 1), EXP-1 is performed with the same grid configuration and numerical set up employed in the control run, but without the Atlas Mountains.[1]

To understand the evolution of the vortex once it emerges from the African continent to the Mediterranean Sea (phase 2) we performed the following experiments: as in the control run, EXP-2 starts at 0000 UTC 24 September 2006 but runs for only 48 h. The model setup is the same as that of the control run except for the horizontal grid system employed. EXP-2 includes two grids: the coarse is the same used in the control run (G1, in Fig. 2) while the inner grid, with 4-km resolution, has 137 × 121 grid points and covers the region between the coast of Tunisia and the southern Sicily (G2b in Fig. 2). This simulation was designed to provide

[1] Initial and boundary conditions are those provided by ECMWF fields at all pressure levels (including those below mountains) interpolated onto the WRF model vertical levels, which have been modified after setting the height of the orography to zero over Africa.

a finer-resolution analysis of the cyclone during phase 2. To explore the role of latent heat release in this phase, EXP-3 is performed. This new simulation is a restart from EXP-2, starting at 0000 UTC 25 September, and run for 24 h; the boundary conditions on G1 are provided, as in the other experiments, by the ECMWF analyses. Grids and numerical setup in EXP-3 are the same as in EXP-2, but the latent heating is turned off. The differences in the MSLP between EXP-3 and EXP-2 can then be attributed only to the absence of latent heating during the passage of the cyclone over the Mediterranean Sea. (If we had suppressed the latent heat from 0000 UTC 24 September onward, the possible changes in MSLP could have also been attributed to changes occurring during the earlier phase when the cyclone was still over the African continent.) EXP-4 is identical to EXP-3, but with the surface heat and moisture fluxes, instead of the latent heating, set to zero.

To test the roles of latent heating and surface fluxes during the time of intensification and transit across the Ionian Sea (phase 3), EXP-5 and EXP-6 were performed. Both experiments are restart runs with the initial fields provided by the control run at 0000 UTC 26 September. The two simulations last for 24 h and the setup is the same as the control experiment. EXP-5 is performed turning off the latent heat release, while in EXP 6, the surface heat and moisture fluxes are turned off.

To study the sensitivity of the cyclone to surface fluxes and to latent heat release when the vortex passes over the Adriatic Sea (phase 4), two additional restart experiments were done: EXP-7 and EXP-8. These experiments are initialized at 0600 UTC 26 September, using as the initial condition the control run 54 h after its starting time. As with the previous two simulations, their configuration is the same as the control run and they are performed turning off first the latent heating (EXP-7) and, then, the surface fluxes (EXP-8).

c. Results of the sensitivity simulations: Phase 1

As shown in the control run, the cyclogenesis of the small-scale vortex seems to be induced by the flow over the Atlas Mountains. To further support this result, the Atlas Mountains have been removed in EXP-1. Figure 7 shows the mean sea level pressure field and the wind at 850 hPa as simulated in EXP-1 at 1800 UTC 24 September (Fig. 7a) and 1200 UTC 25 September (Fig. 7b). By comparing Figs. 6a,b and Figs. 7a,b, it is apparent that initially the pressure minimum is still present (Fig. 7a), although shifted to the north and with a reduced depth with respect to that of the control run (Fig. 6a); however, it completely disappears in 18 h (Fig. 7b), leaving only a wide trough associated with the synoptic low over the northern Tyrrhenian Sea. This result reinforces the interpretation that the cyclone, which became a tropical-like vortex over southern Italy, originates as an orographic vortex on the lee side of the Atlas Mountains.

d. Results of the sensitivity simulations: Phase 2

After its generation, the small-scale cyclone moves eastward, reaching the Mediterranean Sea at about 0600 UTC 25 September and then moving farther eastward toward southern Sicily. The mechanisms involved in the deepening of the cyclone during its transit over the Strait of Sicily are explored in EXP-2; in particular, Fig. 8 shows the time evolution of the 1000-hPa potential temperature, the 10-m horizontal wind vector (Figs. 8a,c,e), and the MSLP and 800-hPa rainwater content (Figs. 8b,d,f) during phase 2. As shown in Fig. 8a, on the inner grid at 0900 UTC 25 September, there is a low-level cyclonic circulation over the Mediterranean Sea, centered offshore of the southeastern coast of Tunisia, where the pressure minimum has the value of about 1008 hPa (Fig. 8b). The horizontal distribution of the potential temperature field evidences the advection of warm air coming from the south on the east side of the cyclone, and the presence of a cold front, extending in the northwestern corner of the grid, from the northeastern coast of Tunisia to western Sicily (Fig. 8a). Along the front, precipitation is generated, as revealed by the distribution of rainwater content at 800 hPa (Fig. 8b).

At 1200 UTC 25 September, Fig. 8c shows that the cold front moves east-southeastward, while the vortex moves northeastward; thus, the two features move closer to each other, and the cyclonic circulation interacts more closely with the cold air following the frontal system on the north and western side of the cyclone. While the minimum pressure value remains almost constant, a smaller-scale minimum forms to the southwest of Sicily as a consequence of the convection operating along the front (Fig. 8d). With respect to 3 h earlier, the convective activity is now more intense as evidenced by the fact that the rainband is longer and the rain content greater (Fig. 8d). At 1800 UTC 25 September, Figs. 8e,f show that the orographically generated cyclone has merged with the smaller-scale convectively produced low, with the latent heat release associated with the convective activity apparently leading to the contraction and intensification of the vortex.

To understand in more detail the model-produced cumulus convection, vertical profiles of wind, temperature, and dewpoint are shown in Fig. 9. The simulated soundings are taken at a few points, the locations of

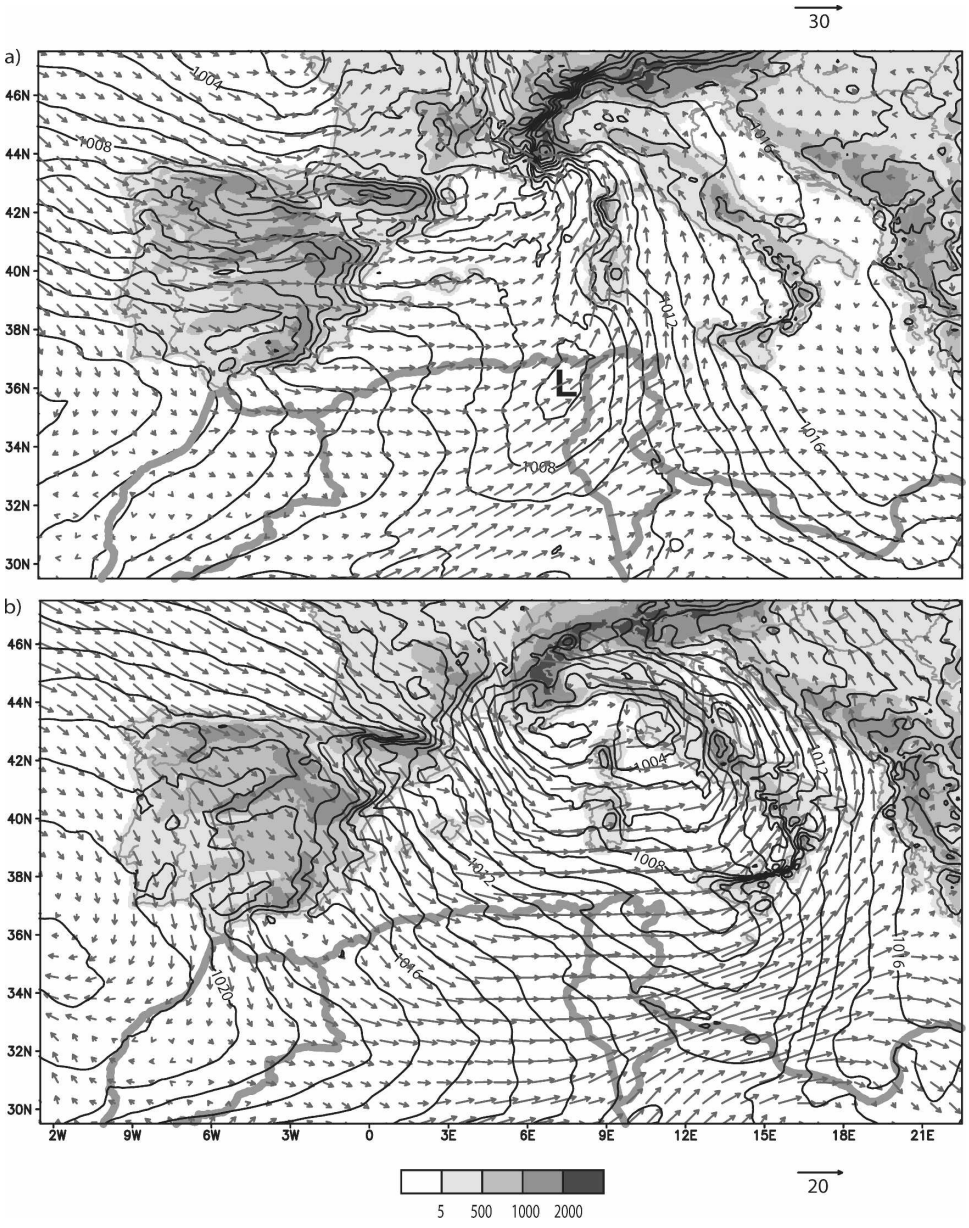

FIG. 7. Sensitivity experiment without the Atlas Mountains (EXP-1). coarse grid: MSLP (black contours, CI = 1 hPa) and 850-hPa horizontal wind component (gray arrows) at (a) 1800 UTC 24 Sep and (b) 12 UTC 25 Sep. The 850-hPa wind speed is proportional to the length of the arrows: the unit length is indicated and is equal to 30 m s^{-1} in (a) and 20 m s^{-1} in (b).

which are indicated by the crosses in Figs. 8b,d,f. These locations were selected in order to represent the changes of the thermodynamic properties of the atmosphere during the passage of the cyclone over the Strait of Sicily.

Figure 9a illustrates the characteristics of the air column above the pressure minimum, in the warm sector of the frontal system, at 0900 UTC 25 September (the "X" in the SW quadrant of Fig. 8b). One can see the strong thermodynamic disequilibrium between the middle-tropospheric cold air and the low-level warm air, which is responsible for the large value of CAPE (3276 J kg^{-1}). However, such instability cannot be released as a consequence of the strong inversion in the low levels of the sounding [convective inhibition (CIN) = 157 J kg^{-1}] because of the presence of a layer of very warm and dry air advected from the African continent by the prevailing southwesterly flow.

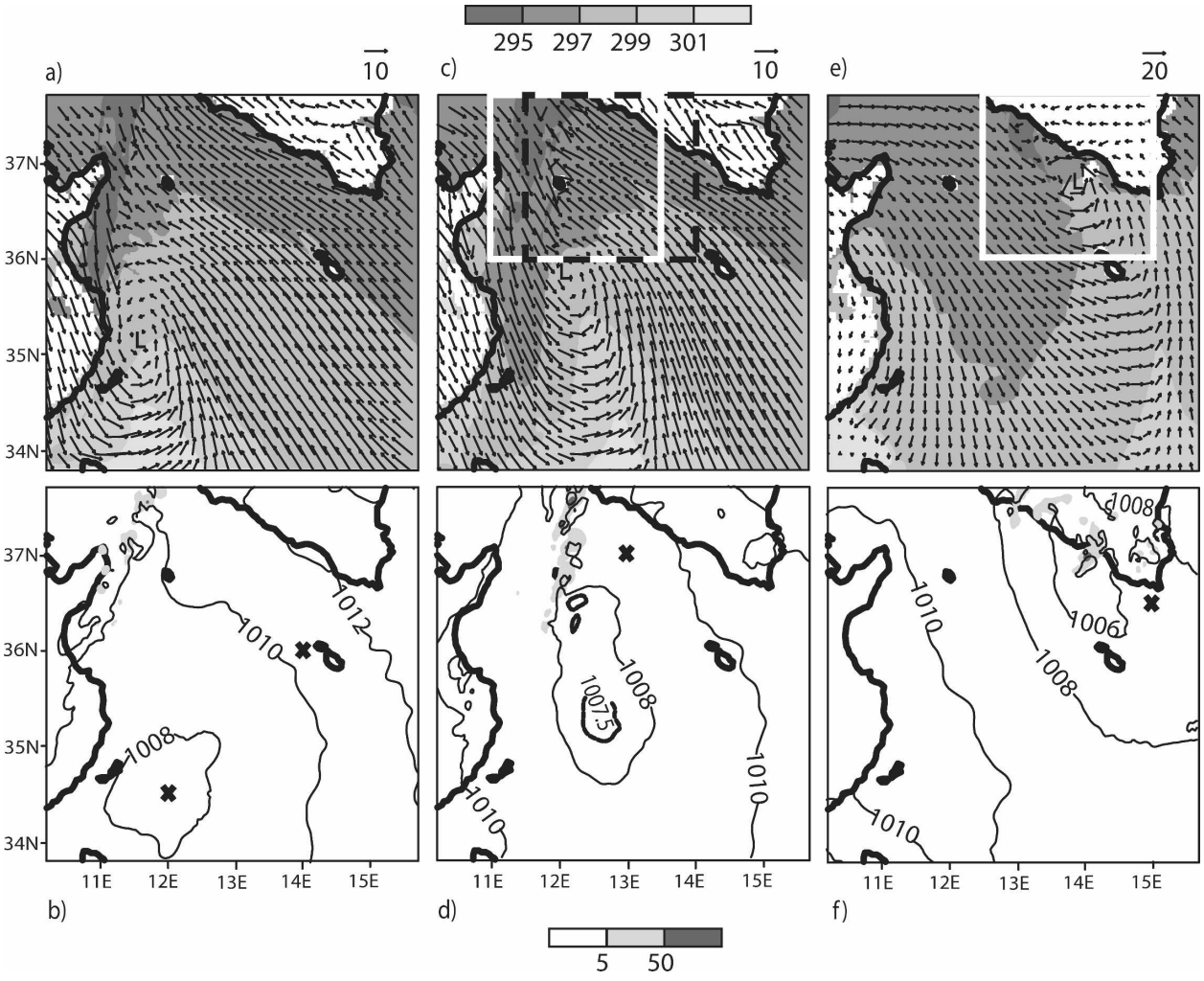

FIG. 8. EXP-2 (inner grid): 1000-hPa potential temperature (K, grayscale-shaded areas) and 10-m horizontal wind (black arrows) at (a) 0900, (c) 1200, and (e) 1800 UTC 25 Sep; 800-hPa rainwater (g kg^{-1}; grayscale-shaded areas); and MSLP at (b) 0900, (d) 1200, and (f) 1800 UTC 25 Sep [black contours, CI = 1 hPa; dashed contour for MSLP = 1007.5 hPa in (d) to better locate the position of the minimum]. The "X" in (b), (d), and (f) denotes the positions where the thermodynamic soundings in Fig. 9 are taken: in particular, the southwestern (northeastern) cross in (b) corresponds to the location of the sounding shown in Fig. 9a (Fig. 9b); the cross in (d) [(f)] corresponds to Fig. 9c (Fig. 9d). The 10-m wind speed is proportional to the length of the arrows: the unit length is shown on the top-right side of each panel and is equal respectively to 10 m s^{-1} in (a) and (c), and 20 m s^{-1} in (e). The grayscale for 1000-hPa potential temperature in (a), (c), and (e) is shown at the top of the figure. The white squares in (c) and (e) represent the domains shown, at the same time, in Figs. 10a and 10c, respectively; the black dashed square in (c) represents the domain shown in Fig. 10b.

At the same time, about 200 km farther away from the cyclone, the sounding shown in Fig. 9b (the "X" in the NE quadrant of Fig. 8b) shows that the low-level southeasterly flow brings air from the southern Mediterranean Sea that is cooler and has a much higher humidity content compared to the air advected toward the center of the cyclone (Fig. 9b versus Fig. 9a). As a consequence, the value of CAPE is smaller (1903 J kg^{-1}). Although the atmosphere is unstable, the advection of warm air from the African continent from the southwest in the low levels is responsible for the deep low-level inversion from about 925 to 825 hPa, which also prevents the release of convection in this region (CIN = 164 J kg^{-1}).

At 1200 UTC 25 September, as the vortex moves closer to the cold front, the characteristics of the air involved in the cyclonic circulation change. The mechanism that modifies the environment is a combination of the uplift induced by the frontal system, which is responsible for the cooling in the low levels, and the latent heat fluxes, which moisten the boundary layer. As a consequence, the sounding extracted on the north side of the vortex, about 70 km to the east of the front (Fig. 9c, marked by the "X" in Fig. 8d), shows, as com-

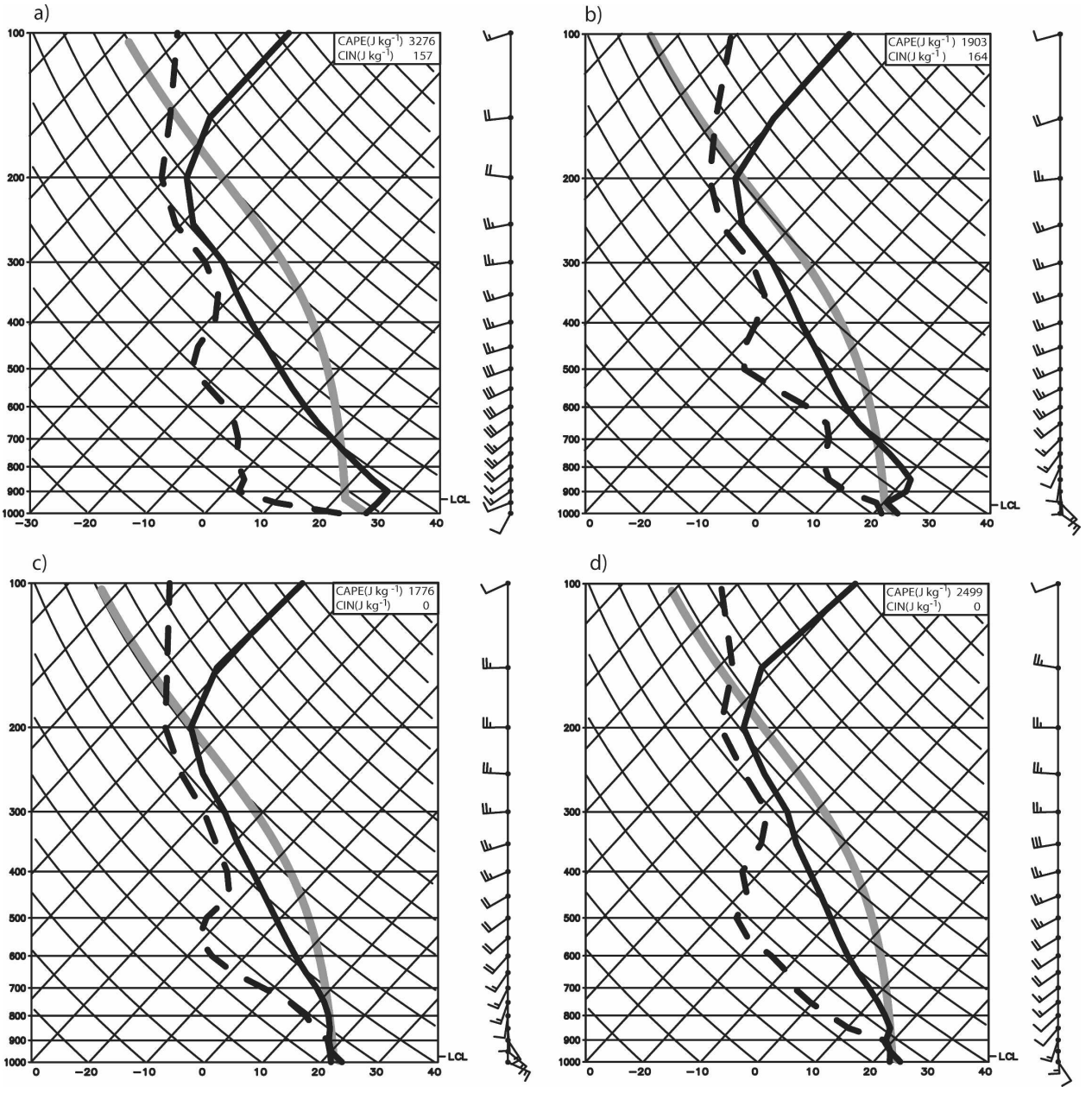

FIG. 9. EXP-2 (inner grid): Thermodynamic soundings at (a) 34.5°N, 12.0°E and (b) 36.0°N, 14.0°E at 0900 UTC 25 Sep; at (c) 37.0°N, 13.0°E at 1200 UTC 25 Sep; and at (d) 36.5°N, 15.0°E at 1800 UTC 25 Sep. The gray solid line represents the thermodynamic path of a parcel lifted from the surface. Wind plotting follows the standard convention (1 small barb = 5 kt; 1 long barb = 10 kt).

pared to Figs. 9a,b, that the air in the low levels is cooler and mostly saturated, and the profile in the 1000–750-hPa layer is nearly moist neutral. The fact that the inversion shown in the previous stage has been eliminated (CIN = 0) and the CAPE is large (1776 J kg^{-1}) indicates conditions favorable to the release of convective instability.

Finally, at 1800 UTC 25 September, when the cold front phases with the orographic cyclone, the air ahead of the front advects from the south, producing a slight temperature increase at low levels with respect to 3 h earlier (cf. Figs. 9c,d). As a consequence, the CAPE increases (2499 J kg^{-1}) while there is still no temperature inversion in the low levels (Fig. 9d).

In conclusion, the time evolution of the vertical profiles ahead of the frontal system shows that the environmental conditions become more favorable for the development of convection as the cyclone moves closer

to the frontal system. At the same time, the convective activity favors the further deepening of the pressure minimum. To better understand the interaction between the front and the orographic vortex, the 1-h difference in MSLP and in 500-hPa potential temperature fields have been analyzed. Figure 10 shows these differences at three distinct time intervals: from 1200 to 1300 UTC (Fig. 10a), from 1400 to 1500 UTC (Fig. 10a), and from 1700 to 1800 UTC (Fig. 10c). The different panels show that, as the front moves to the east along the southwestern coast of Sicily, the 500-hPa temperature field increases (by more than 3°C h^{-1}; not shown) ahead of the front and decreases by a similar amount behind it (not shown); as a consequence, an MSLP decrease up to 4 hPa h^{-1} and an increase up to 3 hPa h^{-1} are observed, respectively, ahead and behind of the frontal line. Although the cooling is due to the advance of the cold air from the northwest, the temperature increase is mainly a consequence of latent heat released during the convective processes. The relevance of this temperature increase for the intensification of the vortex during the afternoon of 25 September is further emphasized with the sensitivity experiments EXP-3 and EXP-4 defined above.

In EXP-3, the diabatic heating from condensation is turned off in the microphysics: as a consequence, convective cells do not develop and the interaction of the orographic vortex with the cold front is not able to deepen the pressure minimum (not shown). In fact, the pressure minimum deepens only 1 hPa in the period from 0600 to 1800 UTC 25 September, when it reaches the value of 1007 hPa (instead of 1003 hPa, as simulated in EXP2). In EXP-4 the latent and sensible heat fluxes from the surface are switched off: Fig. 11 shows the MSLP field at 0900 (Fig. 11a), 1200 (Fig. 11b), and 1800 UTC (Fig. 11c) 25 September. It is apparent that, in contrast with EXP-2 (Fig. 8), the pressure minimum does not decrease as much and the cyclone track is modified, as the system moves over the sea from west-southwest to east-northeast without approaching the coast of Sicily. Since the pressure minimum decrease is similar to EXP-3, we can conclude that the latent heating and the surface fluxes are similarly important in the deepening of the cyclone during phase 2.

The effect of the suppression of the surface fluxes on the thermodynamic properties of the atmosphere is more apparent in Fig. 12, where the vertical profile at 1200 UTC 25 September is plotted in a point located 100 km northeast of the position of the pressure minimum, far ahead of the frontal system (marked by the "X" in Fig. 11b). We compare this sounding with those shown in Figs. 9b,c, which are representative of the

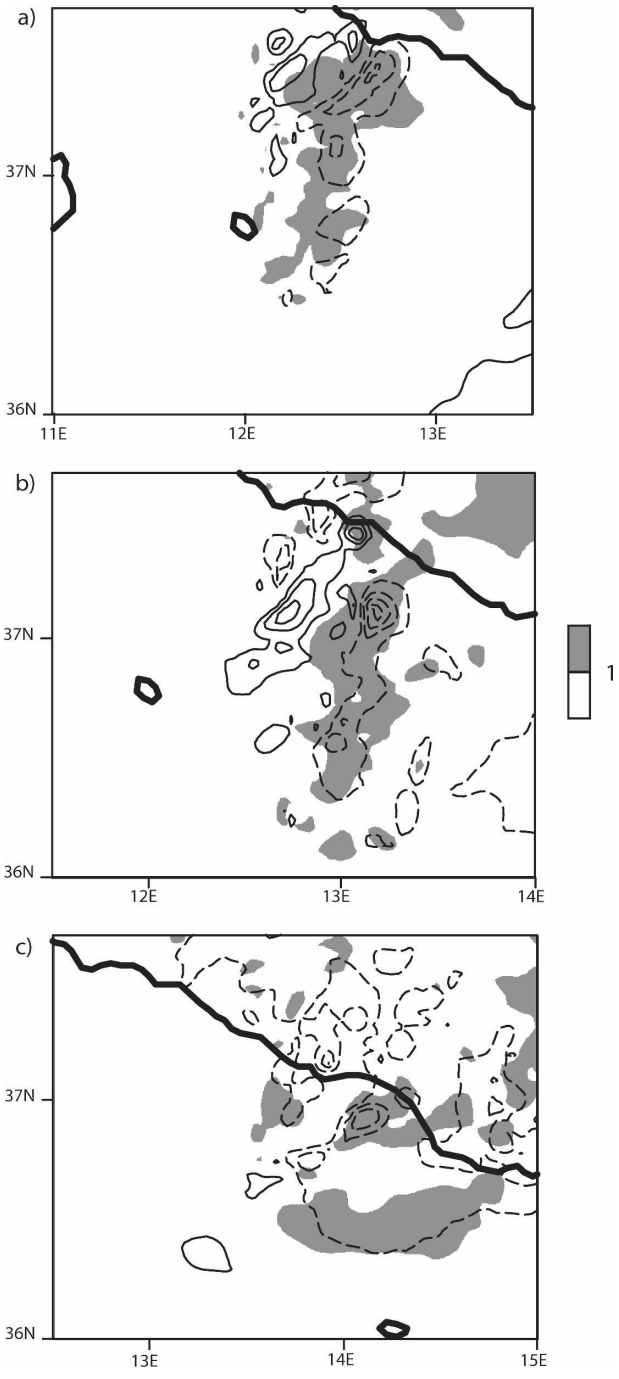

FIG. 10. EXP-2 (inner grid): difference in MSLP (solid contours for positive values; dashed contours for negative values; CI = 1 hPa) and in 500-hPa potential temperature (K, grayscale-shaded areas) fields between (a) 1200 and 1300 UTC, (b) 1400 and 1500 UTC, and (c) 1700 and 1800 UTC 25 Sep, focused on the Mediterranean Sea, to the southwest of Sicily.

atmosphere upwind of the front in EXP-2, at times when the frontal system and the vortex are quite far from each other. We observe that the elimination of surface fluxes reduces the humidity in the low levels

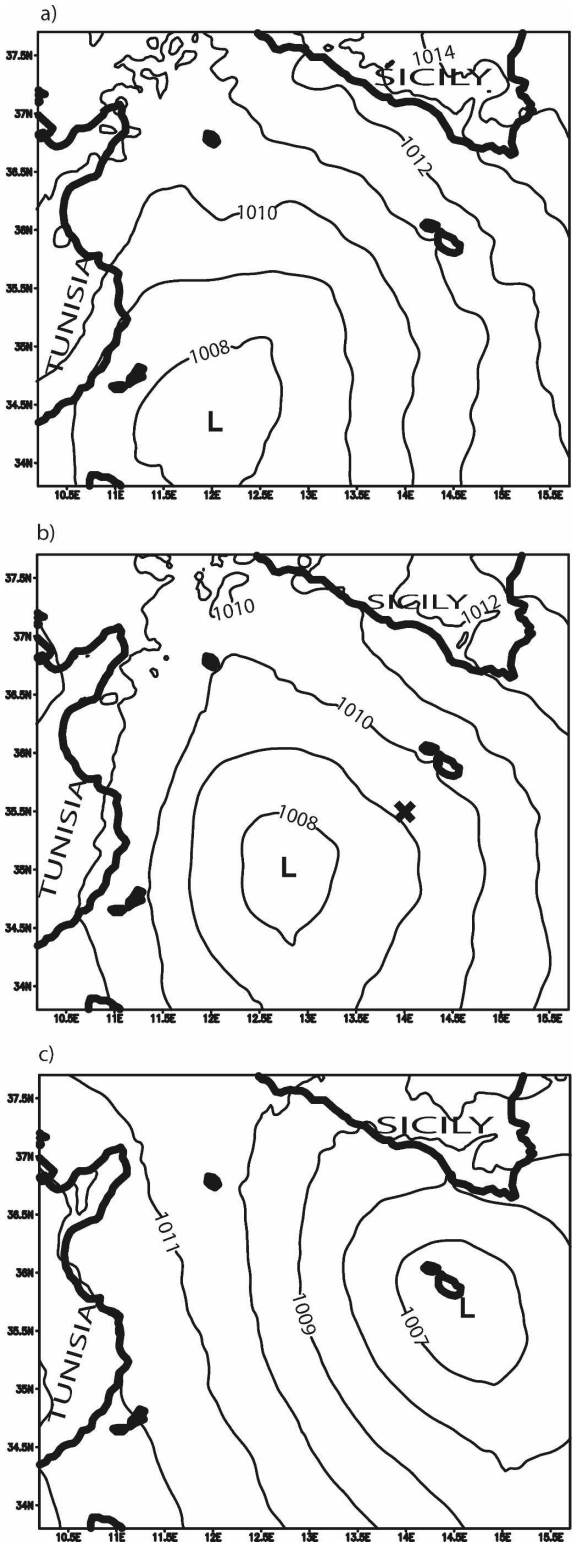

FIG. 11. EXP-4 (sensitivity experiment with heat and moisture surface fluxes turned off; inner grid): MSLP (black contours, CI = 1 hPa) at (a) 0900, (b) 1200, and (c) 1800 UTC 25 Sep. The black cross in (b) shows the position where the thermodynamic sounding in Fig. 12 is taken.

and hence reduces the potential for convection through the domain. The absence of convective reinforcement of the front (and attendant frontal lifting), as illustrated in Figs. 8–10, allows the temperature inversion to persist (CIN = 393 J kg^{-1}) and the instability to be much weaker (CAPE = 197 J kg^{-1}) as shown in Fig. 12. Thus, the atmosphere is no longer favorable to the development of convection and hence the convective intensification and contraction of the vortex does not occur in this simulation.

In conclusion, several mechanisms are important during phase 2: the frontal system, which favors the triggering of convection and enhances the surface fluxes in the vicinity of the vortex, through increased low-level winds and lapse rates; the frontal uplift contributing to the destabilization of the environment and favoring the release of convection in the region; and the latent heat released from convection, which further induces cyclogenesis through diabatic heating over a deep column and is responsible for the contraction of the horizontal extent of the vortex, as simulated by the model in EXP-2. The transition of the relatively large orographically generated cyclone into a much smaller-scale vortex through the action of convection is a complex process and is beyond the scope of the present study. We note that, even in the field of tropical cyclogenesis research, the means by which deep convection transforms a weakly rotating flow into a tropical cyclone is the subject of active current research, but some parallels can be seen with the evolution observed in Fig. 8 and the "hot tower" hypothesis for tropical cyclogenesis (Montgomery et al. 2006).

e. Results of the sensitivity simulations: Phase 3

EXP-2 shows that the vortex crosses southern Sicily during the night of 25 September (not shown) and then enters the Ionian Sea with a minimum pressure value of 1002 hPa; this result is consistent with that of the control run. The movement of the cyclone in the following hours, as simulated in the inner grid of the control run, is illustrated in Fig. 13. At 0300 UTC 26 September, the vortex is over the central part of the Ionian Sea, close to the coast of Calabria, and its MSLP minimum is 997 hPa (Fig. 13a). In just a few hours, the pressure minimum decreases significantly, while the cyclone moves north-northeastward: at 0600 UTC, the vortex is located over the northern Ionian Sea, to the southwest of the Salentine peninsula, with a MSLP minimum of 990 hPa (Fig. 13b). At this time, the system acquires the characteristics typical of a tropical storm: the strong pressure gradient in a small horizontal distance, the existence of a warm core (as shown later in Fig. 18), and

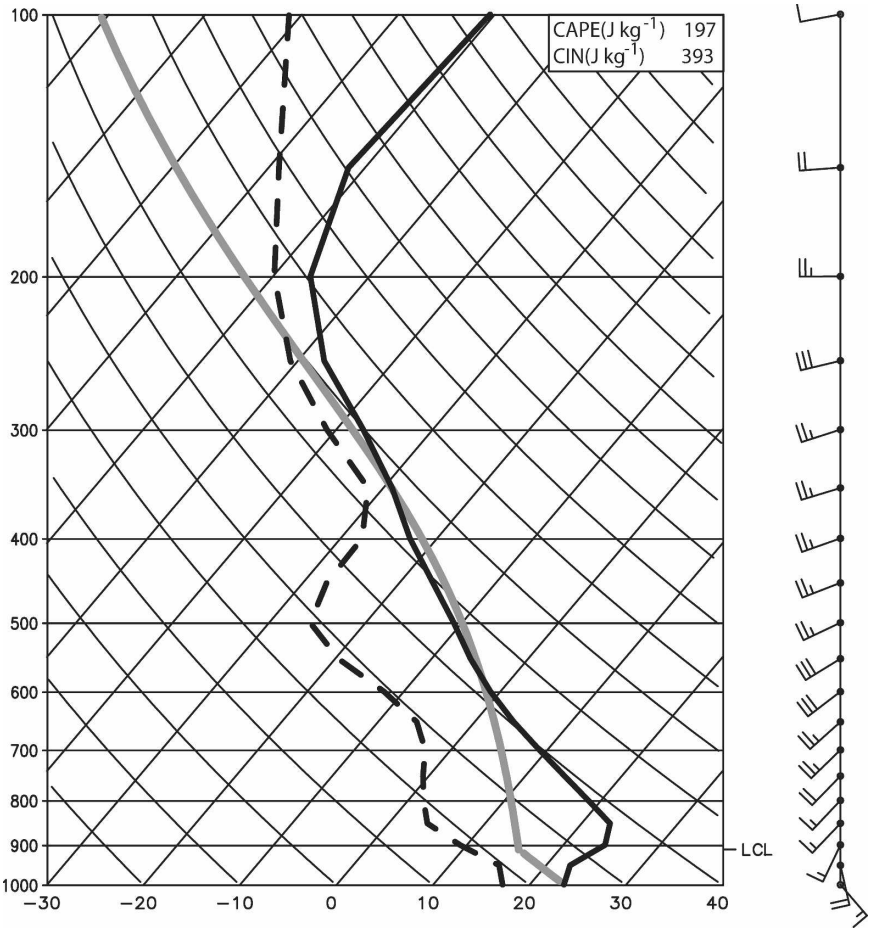

FIG. 12. EXP-4. Inner grid: thermodynamic sounding taken at 35.5°N, 14.0°E at 1200 UTC 25 Sep. The gray solid line represents the thermodynamic path of a parcel lifted from the surface.

the presence of a spirally distributed cloud band around the eye and a cloud-free area in its center.

To investigate the thermodynamic state of the atmosphere in this phase, Fig. 14 shows the vertical profile at 0600 UTC 26 September, about 150 km to the southeast of the pressure minimum, slightly ahead of the convective band. The humidity profile is very close to saturation near the ground, but becomes progressively drier moving to the middle troposphere. The temperature sounding remains close to the pseudoadiabatic profile over the whole troposphere but is slightly unstable (CAPE = 943 J kg^{-1}), while there is no convective inhibition in the low levels: these conditions are typical of a tropical environment prone to tropical cyclone development and have already been observed in the other subsynoptic vortices over the Mediterranean Sea (Rasmussen and Zick 1987).

To investigate the role played by the surface fluxes and the latent heat release in this phase, two additional numerical experiments are performed (EXP-5 and EXP-6). The main results are illustrated in Fig. 15, which shows the MSLP and the 800-hPa rainwater fields at 0300 UTC (EXP-5 and EXP-6, Figs. 15a,c, respectively) and 0600 UTC (EXP-5 and EXP-6 Figs. 15b,d, respectively). By comparing Fig. 15 with the control run results in Fig. 13, it is apparent that the main process that influences the deepening of the vortex over the Ionian Sea is the latent heat release associated with convection. In fact, the evolution of the vortex changes completely by turning off the diabatic heating from condensation (Fig. 15b; EXP-5): Figs. 15a,b show that the pressure minimum value remains almost constant in time, there is no contraction of the horizontal scale of the vortex, and the movement of the cyclone is much slower. Also, the convective band around the cyclone shown in Fig. 13 is completely suppressed. In contrast, the exchanges of sensible and latent heat between the surface and the lower troposphere have a marginal role

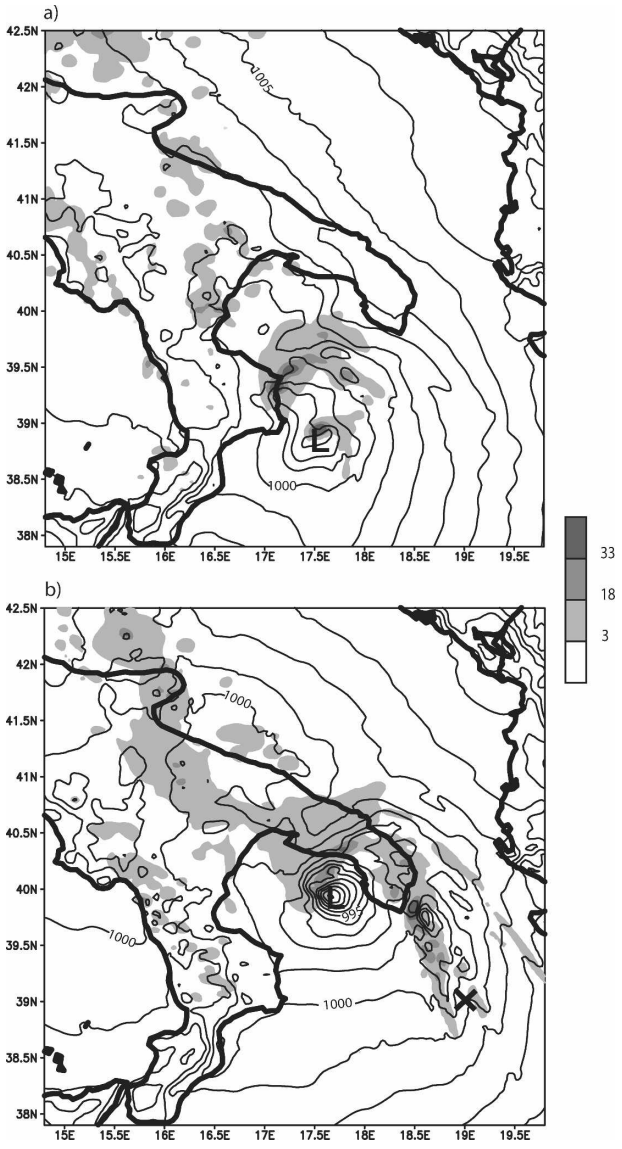

FIG. 13. Control run (inner grid): rainwater (g kg^{-1}) at 800-hPa (grayscale-shaded areas) and MSLP (black contours, CI = 1 hPa) at (a) 0300 and (b) 0600 UTC 26 Sep. The black cross in (b) shows the position where the thermodynamic sounding in Fig. 14 is taken.

in terms of MSLP deepening during this phase. The only effect of turning off the surface fluxes (EXP-6) is an increase of the minimum central pressure of the cyclone by 1–2 hPa with respect to the control run. Also, the convective band around the pressure minimum is still present, although the rainwater content is reduced. Thus, the surface fluxes played a minimal role in phase 3 as the vortex intensifies during its transit over the Ionian Sea; however, since the surface fluxes were necessary in phase 2 to produce the transition from a larger-scale orographically generated cyclone to a smaller-scale hurricane-like vortex and to alter the lower-tropospheric thermal and moisture properties, producing an environment more favorable to the development of convection, they indirectly impacted the cyclone evolution during the subsequent phases.

To understand the mechanisms responsible for the intensification of the diabatic heating associated with convection, and thus of the deepening of the cyclone, we look more closely at the precipitation field (Fig. 16). Intense convective rainfall is simulated to the east of Calabria, along a frontal line moving from the Tyrrhenian to the Ionian Sea. This precipitation occurs ahead of the cyclone, and its hourly intensity in this phase suddenly increases from 60 mm h^{-1} at 0100 UTC 26 September (Fig. 16a) to a maximum of 120 mm h^{-1} at 0300 UTC 26 September (Fig. 16b). This intensification can be ascribed to the interaction of the southeasterly low-level flow, preceding the cyclone, with the steep orography of Calabria (see Fig. 16a). As a consequence, strong uplift develops and generates convection in the area surrounding the cyclone that had become unstable during phase 2. The development of deep convection produces large amounts of latent heat release and warming in the column, and results in a rapid drop of the pressure minimum (7 hPa in only 1 h; see Fig. 3).

Focusing our attention to the east of the Ionian coast of Calabria, the analysis shows that the updrafts are favored by a small-scale cyclogenesis occurring east of the mountains of Calabria, which is downwind with respect to the prevailing westerly midlevel flow. Figure 16a shows that a closed circulation is generated at low levels (mainly confined to the lowest 3000 m) by a mechanism similar to that of the orographic cyclogenesis that occurred south of the Atlas Mountains (see Fig. 6). In a couple of hours, closed isobars develop over the Ionian Sea, to the north of the pressure minimum moving from Sicily (Fig. 16b). During the following hours, the two minima merge and become deeper (not shown).

Since an upper-level potential vorticity (PV) maximum moves close to the vicinity of the vortex in this phase, it would be interesting to evaluate if its role is as relevant for the development of the vortex as in other episodes of Mediterranean tropical-like cyclones (Reale and Atlas 2001; Homar et al. 2003). From our simulations, it turns out that the low-level vorticity structure is already well formed before the passage of the upper-level PV anomaly (not shown), and it is not possible to determine any cause-and-effect relationship between the upper-level PV and the further intensification of the vortex, at least considering the set of experiments performed in the present study.

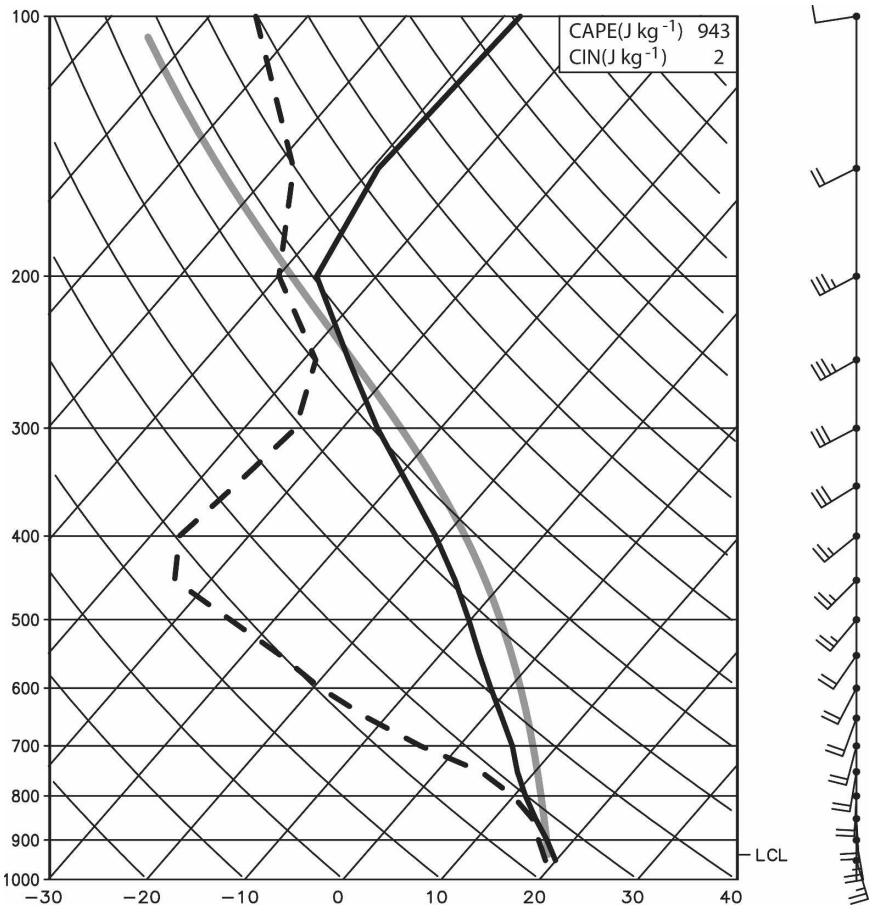

FIG. 14. Control run (inner grid): thermodynamic sounding taken at 39.0°N, 19.0°E at 0600 UTC 26 Sep.

f. Results of sensitivity simulations: Phase 4

Before its ultimate decay, the cyclone moves over the Adriatic Sea. In Fig. 17a, the control run shows that the cyclone is still very deep during this phase, with a minimum value of 990 hPa and a spiral rainwater structure around the eye. To better understand the evolution of the system in this phase, and investigate the importance of latent heating and fluxes, two additional sensitivity experiments are performed; their results are summarized in Figs. 17b,c (EXP-7 and EXP-8, respectively). At 1200 UTC 26 September, the pressure minimum is 995 hPa in EXP-7 and 993 hPa in EXP-8. Thus, the absence of either of the two effects significantly reduces the intensity of the pressure minimum. As a consequence, and in contrast with the previous phase, both the surface heat fluxes and the latent heat release are important in maintaining the strength of the vortex. However, latent heat release still remains the most important mechanism, since EXP-7 reduces the depth of the minimum more than EXP-8 and produces a delay in the temporal evolution of the system, which is not present in EXP-8.

The analogies with the vertical structure of the tropical cyclones during this phase can be better appreciated by considering an azimuthal average of different meteorological fields in a cylindrical coordinate system, the origin of which is coincident with the pressure minimum. Figure 18a represents the vertical cross section of the azimuthally averaged azimuthal wind component (solid contour line) and of the azimuthally averaged potential temperature (shaded areas) fields at 1100 UTC 26 September. A warm core is centered over the surface pressure minimum, with a horizontal extent of about 30 km and a vertical extent through the lower and the middle troposphere (the nonlinear scale used for the vertical coordinate in the figure masks the horizontal temperature gradient at the top of the domain). Associated with this temperature anomaly, there is a cyclonic circulation in the surroundings of the minimum: the azimuthal wind component increases from 0 m s^{-1}, at the center of the

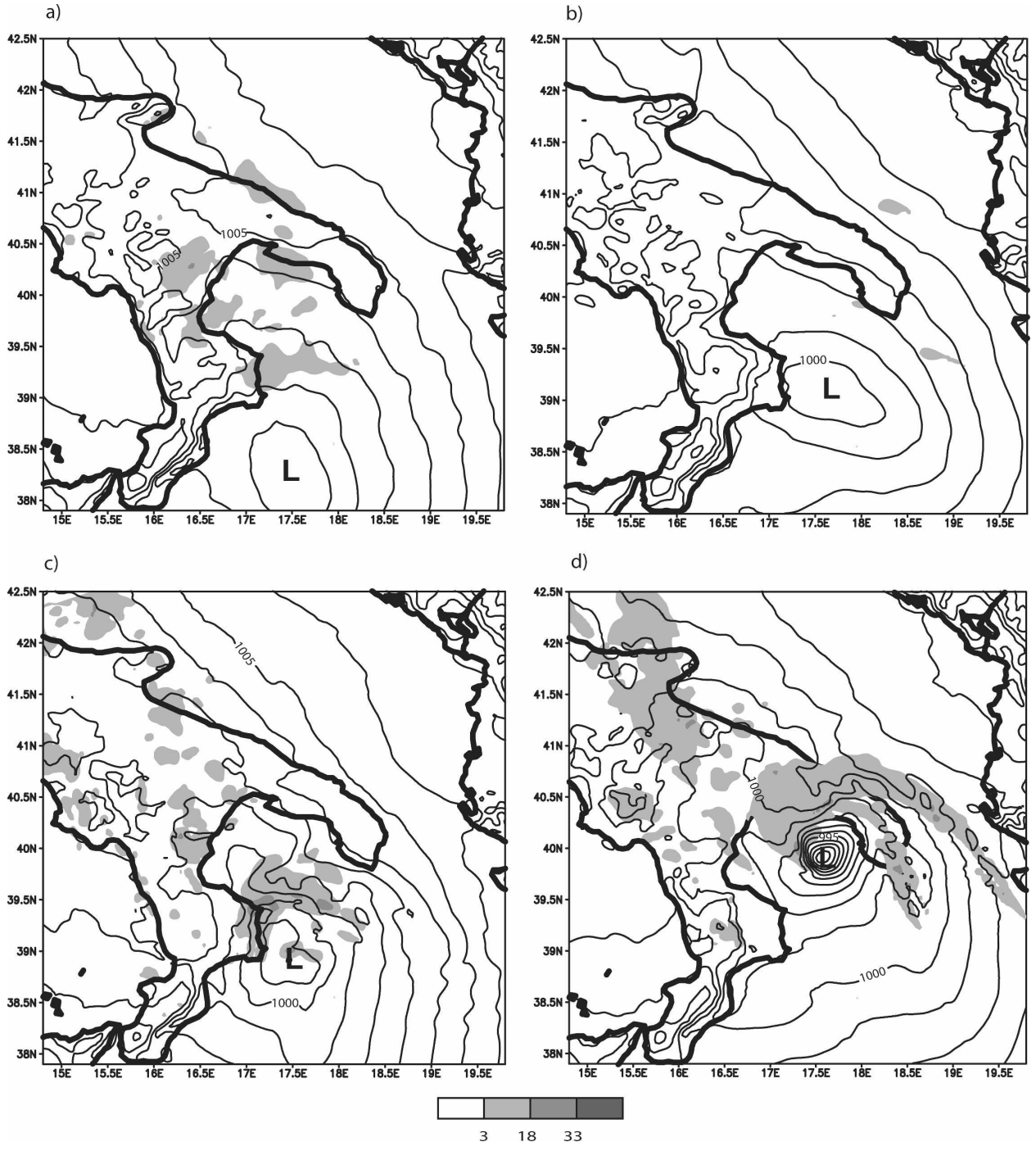

FIG. 15. (a), (b) Sensitivity experiments EXP-5 (with latent heat turned off) and (c), (d) EXP-6 (with heat and moisture surface fluxes turned off). Inner grid: 800-hPa rainwater (g kg^{-1}) content (grayscale-shaded areas) and MSLP (black contours, CI = 1 hPa) at 0300 UTC 26 Sep in (a) and (c) and 0600 UTC 26 Sep in (b) and (d).

pressure minimum, to a maximum of 19 m s^{-1} found close to the ground at a radial distance of about 30 km. This structure reflects the distribution of wind speed (and temperature) typical of tropical cyclones, with a calm eye and a maximum wind speed centered a few tens of kilometers away from the center. A similar velocity distribution was derived by Emanuel (2005) in simulations performed with the nonhydrostatic cloud-resolving model of Rotunno and Emanuel (1987), which, due to its axisymmetric geometry, does

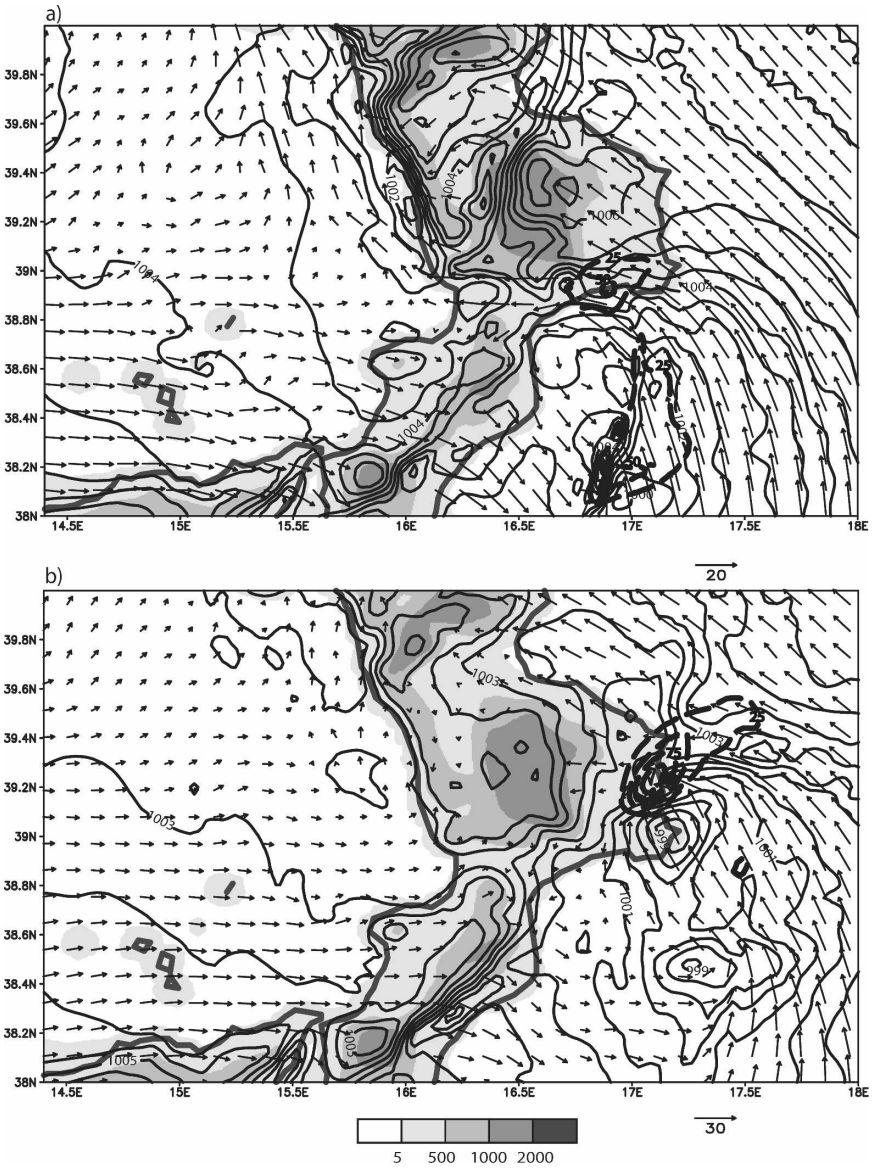

FIG. 16. Control run (inner grid): MSLP (black lines, CI = 1 hPa) and 900-hPa horizontal wind (black arrows) at (a) 0000 and (b) 0200 UTC 26 Sep; hourly rainfall (bolded dashed lines, CI = 25 mm h^{-1}) from (a) 0000 to 0100 UTC 26 Sep and (b) from 0200 to 0300 UTC 26 Sep. The model topography is represented with grayscale-shaded areas. The 900-hPa wind speed is proportional to the length of the arrows: the unit length is shown on the bottom-right side of each panel and is equal to 20 m s^{-1} in (a) and 30 m s^{-1} in (b).

not include baroclinicinstability but only the air–sea interaction processes. Similarly, in our case, after its origin in a baroclinic environment, the vortex assumes tropical cyclone–like features moving over the Adriatic Sea where baroclinicity is not important (not shown).

Figure 18b shows the azimuthal average of the wind vectors resulting from the composition of the radial and vertical components (black arrows) and the azimuthal average of the cloud water mixing ratio in a vertical cross section. As in a tropical cyclone, descending motions are present above the pressure minimum and updrafts are located in the eyewall. There is upward motion, mainly above the area enclosed between 15 and 40 km from the eye, consistent with cloud systems around the core of the cyclone. The distribution of cloud water mixing ratio underscores the presence of a cloud-free area in the center of the cyclone and of convective clouds radially distributed around the center, as for a hurricane.

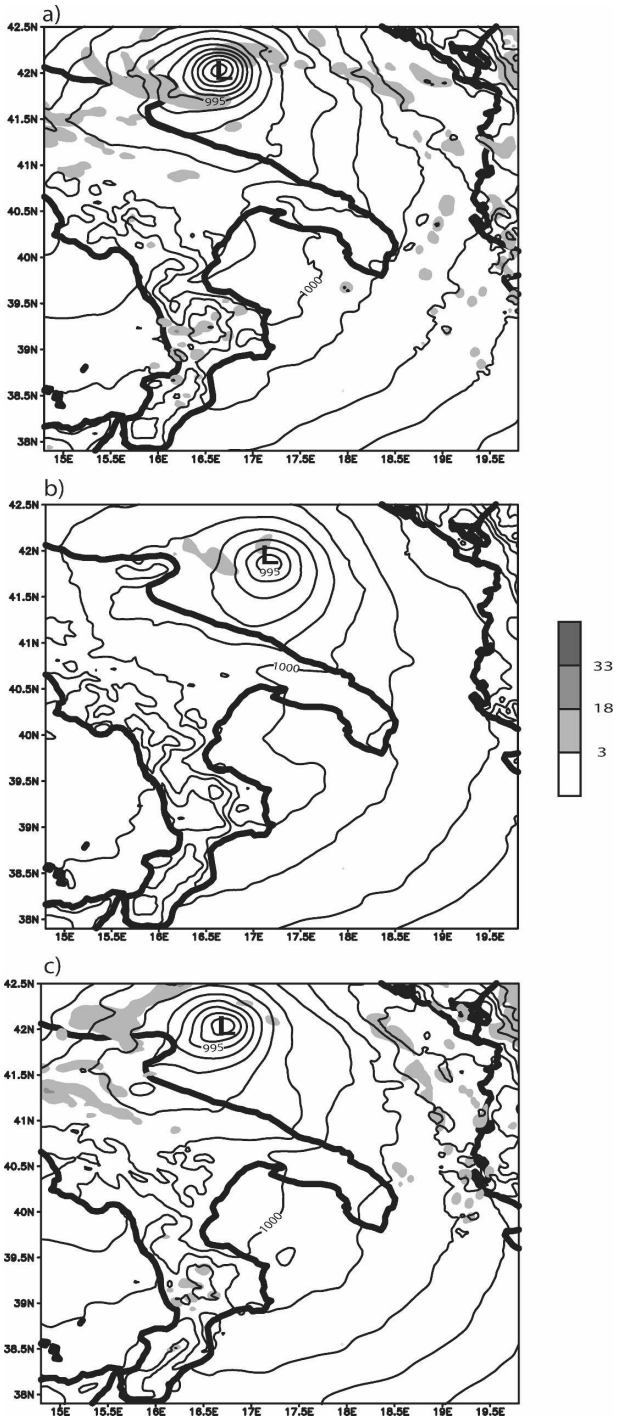

FIG. 17. 800-hPa rainwater (g kg^{-1}, grayscale-shaded areas) and MSLP (black contours, CI = 1 hPa) at 1200 UTC 26 Sep in (a) the control run, (b) EXP-7, and (c) EXP-8.

6. Conclusions

An analysis of a simulation of a small-scale cyclone observed on 26 September 2006 over southeastern Italy and the surrounding area has been presented. The importance of the event can be appreciated by considering that a maximum wind speed of 78 kt was recorded at the Galatina Airport synoptic station, and a minimum sea level pressure of 986 hPa was registered in the area. This value is the lowest in the records of the minimal pressure during similar storms in the Mediterranean area (Fita et al. 2007). The WRF model was used to simulate the evolution of the system and to investigate the leading mechanisms contributing to the genesis, development, and intensification of the small-scale cyclone. By comparing the observed data with the simulations, good agreement is found overall, although a temporal delay of several hours is observed in the evolution of the simulated vortex.

The features of a tropical-like cyclone, such as a warm core, a spiral-like cloud distribution, and high wind speed in the eyewall, are reproduced by the model during the mature phase of the life cycle of the vortex, after the system is well formed over the northern Ionian Sea (from 0600 UTC 26 September onward). The diagnosis of the control run suggests that the evolution of the system can be divided into four different phases: the cyclone formation; the passage of the cyclone over the Mediterranean Sea, along the Strait of Sicily; the transit of the cyclone over the Ionian Sea and its landfall over the Salentine peninsula; and finally the passage of the cyclone over the Adriatic Sea and its landfall in the northern part of Apulia. The different stages of evolution of the cyclone are summarized in Fig. 19.

During the initial phase, a mesoscale depression is generated in the lee of the Atlas Mountains, on 24 September 2006, two days before the event affected Apulia. The system develops in a synoptic environment characterized at 850 hPa by northwesterly flow that enters the Mediterranean Basin and is modified by the northern Africa orography. From its initial appearance at 1200 UTC 24 September and for the following 12 h, the mean sea level pressure minimum neither moves significantly nor does it deepen. Subsequent to this generation phase, the mesoscale cyclone moves eastward and reaches the Mediterranean Sea, east of Tunisia, at 0600 UTC 25 September. In the following phase, the mesoscale cyclone crosses the western Mediterranean Sea and intensifies, as a consequence of its interaction with convection produced along a synoptic-scale cold front moving eastward from the Tyrrhenian Sea. At 0000 UTC 26 September, the now-small-scale cyclone enters the Ionian Sea, where, in the following 6 h, the model simulates a pressure fall of 13 hPa as a consequence of the cyclone's interaction with convection enhanced by the orography of Calabria.

The transition of the extratropical disturbances into tropical cyclones is frequent in the Atlantic tropical ar-

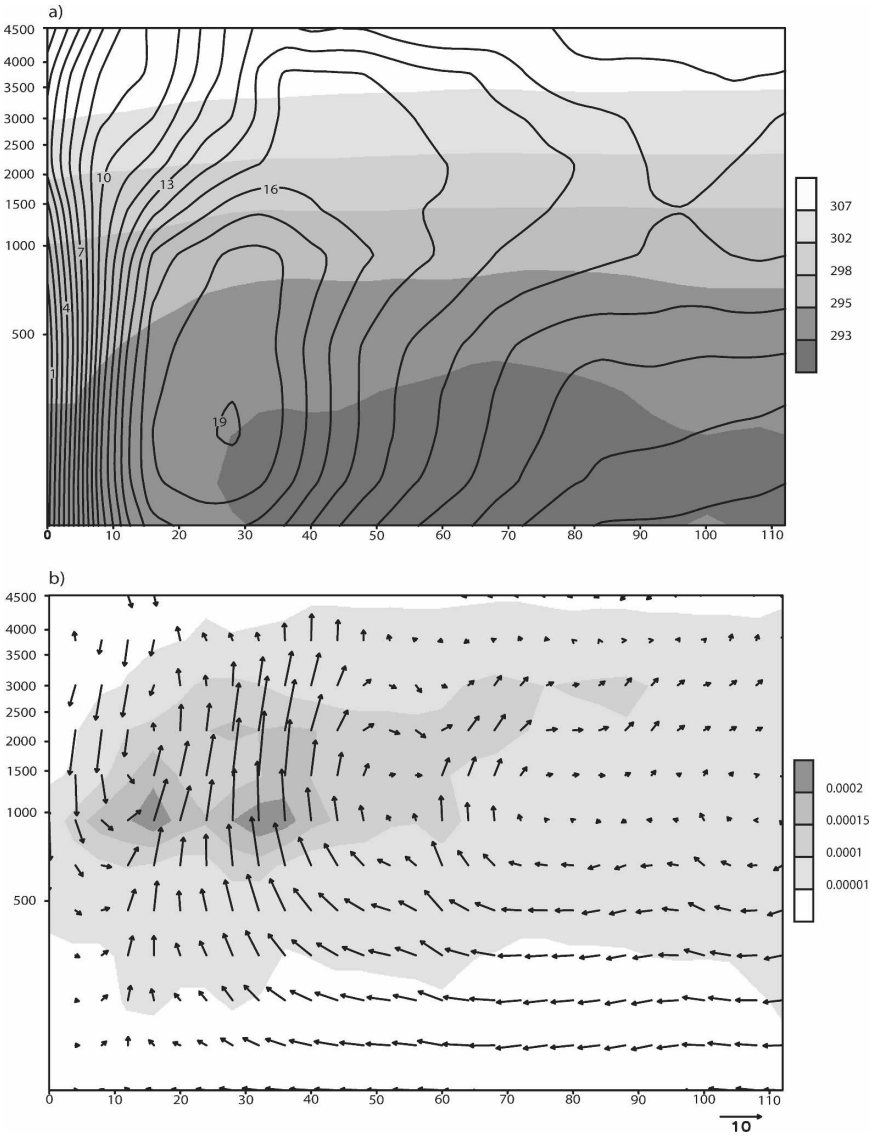

FIG. 18. (a) Vertical cross section of the azimuthal average of the azimuthal wind velocity ($m\ s^{-1}$, black lines) and potential temperature (K, grayscale-shaded areas) at 1100 UTC 26 Sep, in a coordinate system where the origin of the system is located over the pressure minimum; (b) component of the wind vector resulting from the composition of the radial and vertical components (black arrows) and cloud water mixing ratio ($g\ g^{-1}$, grayscale-shaded areas) at 1100 UTC 26 Sep. The horizontal axis represents the radial distance (km) from the center of the pressure minimum; the vertical axis represents the height (m) (the vertical levels of the model are equidistant along the vertical axis; thus, the scale of distances is not linear with respect to the vertical and the numbers on the vertical axis are only approximate, since the model levels are only approximately at a fixed height). The wind speed of the component resulting from the radial and vertical components is proportional to the length of the arrows: the unit length is shown on the bottom-right side of (b) and is equal to 10 $m\ s^{-1}$.

eas (McTaggart-Cowan et al. 2007) and is the subject of active current research. According to the classification of Davis and Bosart (2004) for tropical cyclone development, the cyclone described in the present paper would belong to the weak extratropical cyclones (WEC) category, meaning that the orographically generated low-level cyclone is not capable of self-organized convection. Indeed, an intermediate process is needed to enhance mesoscale vorticity, organize convection, and produce a self-sustaining vortex. In the present

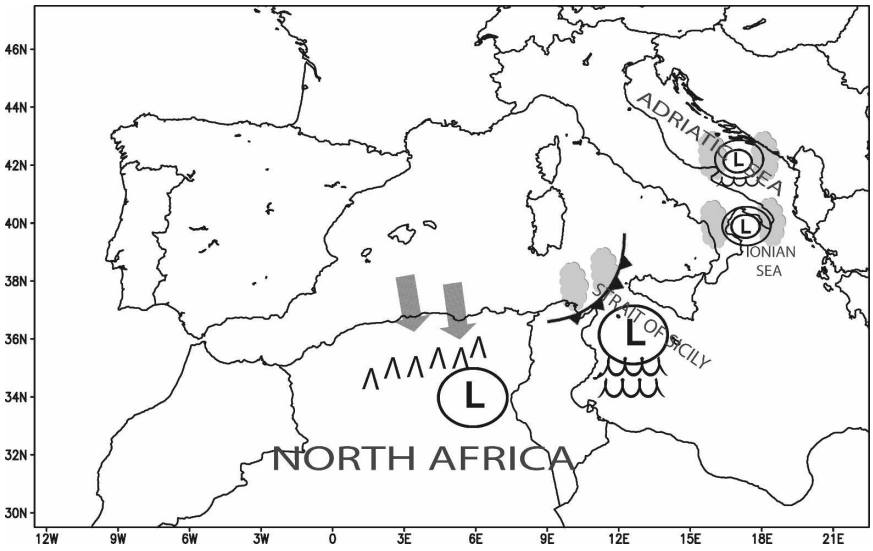

FIG. 19. Summary representing the different stages of evolution of the cyclone. The chain of events leading to the small-scale vortex over southern Italy begins with the action of the northerly flow (gray arrows) impinging on the Atlas Mountains ("Λ" symbols) and producing an orographic cyclone occurring downwind ("L" indicates pressure low). As the orographically produced cyclone moves to the east over the Strait of Sicily, its interaction with a cold-frontal system favors the development of convection (represented by the gray clouds) nourished by sea surface fluxes (represented with the wave symbols). The latter interaction transforms the larger-scale orographic vortex into an intense smaller-scale vortex (represented with the increased number of circles around the "L"), which deepens further due to the convection over the Ionian Sea and is maintained by both convection and sea surface fluxes as it progresses over the Adriatic Sea.

case, the interaction with the synoptic-scale cold front (and the upper-level trough) over the Strait of Sicily and the orographically generated cyclone to the east of Calabria seem to play that role.

In the following hours, the system crosses the Salentine peninsula, where the model simulates the lowest pressure value of 989 hPa near the middle of the peninsula, in good agreement with the observations. After its quick transit over land, the vortex reaches the Adriatic Sea. At this time, the pressure minimum is still deep (990 hPa) and remains constant throughout the vortex's transit over the sea until its second landfall in the northern part of Apulia, where the system finally decays.

Additional numerical simulations were performed to better understand the mechanisms responsible for the genesis and the evolution of the vortex. A numerical experiment without the Atlas Mountains shows that the small-scale intense cyclone that ultimately affected southern Italy originated as an orographic vortex on the lee side of the Atlas Mountains. In the cyclone's subsequent passage over the Mediterranean Sea, the system evolves into a smaller-scale cyclone with high moisture content in the very low levels. Surface heat fluxes and convection are shown to be important during this phase. The surface fluxes are fundamental for the destabilization of the environment, while the latent heat, released within the convective motions that developed near the approaching cold front, is necessary to produce the intensification and contraction of the horizontal scale of the vortex. During its subsequent crossing of the Ionian Sea, the deepening of the now-small-scale vortex is very rapid, and is mainly due to latent heating associated with moist convection, as turning off the latent heat release due to condensation has the effect of delaying and weakening the system development. The results are consistent with those found by Lagouvardos et al. (1999), who stressed the significant role played by the sensible and latent heat fluxes in the formation of a tropical-like Mediterranean storm and the strong influence of the latent heat release due to convective motions, during its mature stage.

In its last stage, the small-scale cyclone crosses the Adriatic Sea. During this phase, both the surface fluxes and the release of latent heat are important in maintaining the strength of the vortex. At this time the system is well formed, and its similarities with tropical cyclones are apparent by azimuthal averages of the wind, potential temperature, and the cloud water content, in a coordinate system where the origin is located

over the pressure minimum. In this last stage, the results are very close to those found in previous studies obtained with theoretical models containing only air–sea interaction processes (Emanuel 2005; Fita et al. 2007).

Finally, several sensitivity experiments were performed to address the predictability of these types of cyclones. Simulations with different initial and boundary conditions were run; also, different limited-area models were used, following a multimodel approach (Davolio et al. 2008, manuscript submitted to *Nat. Hazards Earth Syst. Sci.*). Although most of these simulations were able to reproduce the evolution of the cyclone, a significant sensitivity was found, depending mainly on the large-scale analysis/forecasts and less on the choice of the model. The effects of the initial/boundary conditions will be analyzed further in future work.

Acknowledgments. The visit of R. Rotunno to CNR (Lecce, Italy) in September 2006 was supported by the CNR-Short Term Mobility Program. The visit of A. Moscatello to NCAR was supported by Progetto MIUR "Sviluppo di un Sistema Integrato Modellistica Numerica-Strumentazione e Tecnologie Avanzate per lo Studio e le Previsioni del Trasporto e della Diffusione di Inquinanti in Atmosfera" and CNR-Short Term Mobility Program. The stay of M. Miglietta was in part supported by NCAR.

REFERENCES

Billing, H., I. Haupt, and W. Tonn, 1983: Evolution of a hurricane-like cyclone in the Mediterranean Sea. *Beitr. Phys. Atmos.,* **56,** 508–510.

Buzzi, A., and S. Tibaldi, 1978: Cyclogenesis in the lee of the Alps: A case study. *Quart. J. Roy. Meteor. Soc.,* **104,** 271–287.

Campins, J., A. Jansa, and A. Genoves, 2006: Three-dimensional structure of western Mediterranean cyclones. *Int. J. Climatol.,* **26,** 323–343.

Davis, C. A., and L. F. Bosart, 2004: The TT problem: Forecasting the tropical transition of cyclones. *Bull. Amer. Meteor. Soc.,* **85,** 1657–1662.

——, and M. T. Stoelinga, 1999: Interpretation of the effect of mountains on synoptic-scale baroclinic waves. *J. Atmos. Sci.,* **56,** 3303–3320.

Dyer, A. J., and B. B. Hicks, 1970: Flux-gradient relationships in the constant flux layer. *Quart. J. Roy. Meteor. Soc.,* **96,** 715–721.

Dudhia, J., 1989: Numerical study of convection observed during the Winter Monsoon Experiment using a mesoscale two-dimensional model. *J. Atmos. Sci.,* **46,** 3077–3107.

Emanuel, K. A., 2005: Genesis and maintenance of "Mediterranean hurricanes." *Adv. Geosci.,* **2,** 217–220.

Ernst, J. A., and M. Matson, 1983: A Mediterranean tropical storm? *Weather,* **38,** 332–337.

Fita, L., R. Romero, A. Luque, K. Emanuel, and C. Ramis, 2007: Analysis of the environments of seven Mediterranean tropical-like storms using an axisymmetric, nonhydrostatic, cloud resolving model. *Nat. Hazards Earth Syst. Sci.,* **7,** 41–56.

Homar, V., C. Ramis, and S. Alonso, 2002: A deep cyclone of African origin over the western Mediterranean: Diagnosis and numerical simulation. *Ann. Geophys.,* **20,** 93–106.

——, R. Romero, D. J. Stensrud, C. Ramis, and S. Alonso, 2003: Numerical diagnosis of a small, quasi-tropical cyclone over the western Mediterranean: Dynamical vs. boundary factors. *Quart. J. Roy. Meteor. Soc.,* **129,** 1469–1490, doi:10.1256/qj.01.91.

Hong, S.-Y., and H. L. Pan, 1996: Nonlocal boundary layer vertical diffusion in a medium range forecast model. *Mon. Wea. Rev.,* **124,** 2322–2339.

Kain, J. S., 2004: The Kain–Fritsch convective parameterization: An update. *J. Appl. Meteor.,* **43,** 170–181.

Lagouvardos, K., V. Kotroni, S. Nickovic, D. Jovic, and G. Kallos, 1999: Observations and model simulations of a winter subsynoptic vortex over the central Mediterranean. *Meteor. Appl.,* **6,** 371–383.

McTaggart-Cowan, R., L. F. Bosart, J. R. Gyakum, and E. H. Atallah, 2007: Hurricane Katrina (2005). Part I: Complex life cycle of an intense tropical cyclone. *Mon. Wea. Rev.,* **135,** 3905–3926.

Michalakes, J., J. Dudhia, D. Gill, T. Henderson, J. Klemp, W. Skamarock, and W. Wang, 2004: The Weather Research and Forecast Model: Software architecture and performance. *Proc. 11th Workshop on the Use of High Performance Computing in Meteorology,* Reading, United Kingdom, ECMWF, 156–168.

Mlawer, E. J., S. J. Taubman, P. D. Brown, M. J. Iacono, and S. A. Clough, 1997: Radiative transfer for inhomogeneous atmosphere: RRTM, a validated correlated-k model for the longwave. *J. Geophys. Res.,* **102** (D14), 16 663–16 682.

Montgomery, M. T., M. E. Nichols, T. A. Cram, and A. B. Saunders, 2006: A vortical hot tower route to tropical cyclogenesis. *J. Atmos. Sci.,* **63,** 355–386.

Moscatello, A., M. M. Miglietta, and R. Rotunno, 2008: Observational analysis of a Mediterranean "hurricane" over southeastern Italy. *Weather,* in press.

Paulson, C. A., 1970: The mathematical representation of wind speed and temperature profiles in the unstable atmospheric surface layer. *J. Appl. Meteor.,* **9,** 857–861.

Pierrehumbert, R. T., 1984: Lee cyclogenesis. *Mesoscale Meteorology and Forecasting,* P. D. Ray, Ed., Amer. Meteor. Soc., 493–515.

Pytharoulis, I., G. C. Craig, and S. P. Ballard, 2000: The hurricane-like Mediterranean cyclone of January 1995. *Meteor. Appl.,* **7,** 261–279.

Rasmussen, E., and C. Zick, 1987: A subsynoptic vortex over the Mediterranean with some resemblance to polar lows. *Tellus,* **39A,** 408–425.

Reale, O., and R. Atlas, 2001: Tropical cyclone–like vortices in the extratropics: Observational evidence and synoptic analysis. *Wea. Forecasting,* **16,** 7–34.

Romero, R., 2001: Sensitivity of a heavy rain producing western Mediterranean cyclone to embedded potential vorticity anomalies. *Quart. J. Roy. Meteor. Soc.,* **127,** 2559–2597.

Rotunno, R., and K. Emanuel, 1987: An air–sea interaction theory

for tropical cyclones. Part II: Evolutionary study using a nonhydrostatic axisymmetric numerical model. *J. Atmos. Sci.,* **44,** 542–561.

Skamarock, W. C., R. Rotunno, and J. B. Klemp, 1999: Models of coastally trapped disturbances. *J. Atmos. Sci.,* **56,** 3349–3365.

——, J. B. Klemp, J. Dudhia, D. O. Gill, D. M. Barker, W. Wang, and J. G. Powers, 2005: A description of the Advanced Research WRF version 2. NCAR Tech. Note 468 STR, 88 pp.

Thompson, G., R. M. Rasmussen, and K. Manning, 2004: Explicit forecasts of winter precipitation using an improved bulk microphysics scheme. Part I: Description and sensitivity analysis. *Mon. Wea. Rev.,* **132,** 519–542.

Webb, E. K., 1970: Profile relationships: The log-linear range, and extension to strong stability. *Quart. J. Roy. Meteor. Soc.,* **96,** 67–90.

Wicker, L. J., and W. C. Skamarock, 2002: Time splitting methods for elastic models using forward time schemes. *Mon. Wea. Rev.,* **130,** 2088–2097.